Representing improved tropospheric ozone distribution over the Northern Hemisphere by including lightning NOx emissions in CHIMERE

Sanhita Ghosh[1], Arineh Cholakian[1], Sylvain Mailler[1, 2], and Laurent Menut[1]

[1]Laboratoire de Météorologie Dynamique, IPSL, École Polytechnique, Route de Saclay, Palaiseau, France, 91128
[2]École des Ponts, Marne-la-Vallée, Institut Polytechnique de Paris

Correspondence: Sanhita Ghosh (ghosh.sanhita@lmd.ipsl.fr; sanhitaghosh027@gmail.com)

Abstract. Estimating nitrogen oxide emissions from lightning (LNOx) in models is highly uncertain, affecting the accuracy of atmospheric composition and air quality assessments. Still, it is essential to include ~~the emissions in model~~ these emissions in models to increase the realism in representing the ~~model outcomes~~gases and aerosols. LNOx emissions have recently been incorporated into the updated version of the CHIMERE model (v2023r2). In ~~the present~~ this study, we evaluate the present state of modelling the lightning flashes ~~and the LNOx emissions~~over the Northern Hemisphere (NH), using a classical scheme based on cloud top height (CTH) and ~~the model CHIMERE. We asses the impact of LNOx on tropospheric ozone (O_3) concentration over the northern hemisphere (NH) through a detailed evaluation of simulated tropospheric O_3. The total NO emission from lightning is estimated as 8.82 Tg N yr^{-1}~~ an updated ice flux-based scheme. We conduct a comprehensive 3D comparison of model outputs, including in situ measurements and satellite data, to rigorously assess the robustness and applicability of these parameterizations. The comparative analysis reveals that the CTH scheme provides a more accurate spatial variability of lightning flashes over lands and tropical oceans. Both parameterizations accurately capture the magnitude of lightning flashes over the tropics, while the ICEFLUX scheme is more effective in representing mid-latitudinal flashes. However, both schemes perform well in capturing the seasonal variation of lightning flashes. The estimated flash frequencies over the NH ~~.~~ from the experiments closely align with satellite observations, and the LNOx emissions fall within the range reported in previous modeling studies. There is an overall increase in ozone (O_3) concentration due to inclusion of LNOx~~. The increase is highest in the mid to upper troposphere, specifically over the tropics. The comparison of the simulated O_3 to measurements shows that the inclusion of LNOx emissions~~ , which substantially improves the tropospheric O_3 distribution, ~~reducing bias significantly. This is particularly true for the free troposphere over the tropical regions~~specifically at the tropical free troposphere. The LNOx emissions hence critically influence the O_3 ~~concentration~~ burden as well as the ~~concentration of~~ hydroxyl radicals (OH)~~. There are 15% and 40% increases, respectively, in O_3 and OH burden as observed due to the inclusion of LNOx in model~~, which further impact the atmospheric lifetime of trace gas methane (CH_4)~~by reducing it by 24%.~~ .

1 Introduction

Nitrogen oxides (NOx), consisting of nitric oxide (NO) and nitrogen dioxide (NO_2), are ~~critical~~ trace gases that play a key role in atmospheric chemistry, particularly in the formation of tropospheric ozone (O_3) (Finney et al., 2014; Luo et al., 2017; Akimoto and Tanimoto, 2022). NOx emissions arise from both anthropogenic sources~~(~~, e.g., fossil fuel combustion, biomass burning~~) ,~~ and natural processes, such as lightning and soil-NOx emissions (Verma et al., 2021; Butler et al., 2020). Among these sources, lightning-induced NOx (LNOx) contributes approximately 10%–15% to global NOx emissions, with an even greater contribution (up to 70%) in the upper troposphere (Maseko et al., 2021; Luhar et al., 2021; Wu et al., 2023). Importantly, LNOx has a stronger impact on tropospheric O_3 formation compared to surface-based sources, due to the altitude at which LNOx is injected into the atmosphere and the efficiency of O_3 production in the upper troposphere (Finney et al., 2016a; Luhar et al., 2021). ~~However, the~~ The mean estimated rate of NOx emissions ~~due to~~ from lightning is highly uncertain, ~~ranging from 8 mol NO to 4000 mol NO per flash (Finney et al., 2016a; Arndt et al., 2019),~~ with recent studies indicating variations ranging between 33–660 moles NO per flash (Luhar et al., 2021; Bucsela et al., 2019; Murray, 2016; Schumann and Huntrieser, 2007) ; although Schumann and Huntrieser (2007) suggest a mean value of 250 ~~mol~~ moles NO per flash. ~~Nevertheless~~In spite of this uncertainties, inclusion of these emissions in models is essential to enhance the accuracy and reliability of model projections.

The inclusion of LNOx in chemistry-transport models has been ~~the focus of research~~ a research topic for several decades (Kang et al., 2020), with seminal studies by Price and Rind (1992); Price et al. (1997a); Schumann and Huntrieser (2007); Allen et al. (2010); Finney et al. (2014), pioneering the quantification of lightning flash rates and their associated NOx production. These foundational studies laid the groundwork for understanding the contribution of LNOx to tropospheric chemistry (Allen et al., 2010; Banerjee et al., 2014; Finney et al., 2016a; Kang et al., 2019, 2020). A range of parameterization schemes, including diverse empirical equations, have been developed over decades to quantify lightning flash rates and their spatial distribution (Finney et al., 2014). Despite the significant progress made, challenges remain in accurately quantifying LNOx emissions, due to uncertainties in characterizing both the spatial and temporal variations in lightning frequency and intensity, the apportionment among 'cloud to ground (CG)' and 'in cloud (IC)' flashes, the rates of NOx production from lightning discharges, as well as the vertical distribution and transportation of LNOx after its generation (Labrador et al., 2005; Schumann and Huntrieser, 2007; Menut et al., 2020a; Wu et al., 2023). Recent studies have focused on improving the representation of lightning in models through various parameterization schemes ~~, including~~ based on cloud top height ~~(CTH) (Price and Rind, 1992; Price et al., 1997a; Clark et al., 2017)~~(CTH, Price and Rind, 1992; Price et al., 1997a; Clark et al., 2017) , ice flux ~~(Finney et al., 2014)~~(ICEFLUX, Finney et al., 2014), convective precipitation, ~~updraught~~ updraft of mass flux (Allen et al., 2000; Allen and Pickering, 2002) and convective available potential energy ~~(CAPE) (Choi et al., 2005; Zhao et al., 2009)~~ (CAPE, Choi et al., 2005; Zhao et al., 2009). These approaches aim to better capture the spatial and temporal variability of lightning activity, leading to more accurate estimates of LNOx emissions.

In this study, we expand ~~upon~~ on the previous work by ~~utilizing the most frequently used CTH scheme in the CHIMERE~~ implementing the ICEFLUX scheme in chemistry-transport model ~~to evaluate the current state of LNOx modelling. The model CHIMERE was developed in~~ CHIMERE and comparing it with the CTH scheme. The CHIMERE model has been developed

since 1997 and ~~has been~~ modified on a regular basis for better prediction of ~~atmospheric substances~~ trace gases and aerosols (Menut et al., 2020b). The improvement in the natural emissions in the recent version of the model, allows the incorporation of LNOx emissions (Menut et al., 2024). The study by Menut et al. (2020a), conducted over a short period of two months (July–August, 2013), covering Europe and the northern part of Africa, demonstrates changes in tropospheric O_3 and NOx concentrations resulting from the inclusion of LNOx emissions in CHIMERE, using CTH scheme. However, opportunities remain to improve the representation of flash rates ~~by applying correction factors . A comprehensive~~ in the model. To address this, we have applied the recent ICEFLUX parameterization. The CTH scheme does not incorporate the complex interactions and charge distributions that drive lightning production (Price and Rind, 1992; Finney et al., 2014), nor does it account for detailed microphysical processes, storm dynamics, and the presence of ice particles (Price and Rind, 1992). The improved modelling of cloud ice has facilitated the inclusion of the upward flux of ice crystals (Finney et al., 2014). However, ice flux alone is insufficient to fully capture the complexities of lightning phenomena, as additional factors likely influence the charging process. Therefore, a comparative analysis of the traditional CTH and the updated ICEFLUX schemes is essential to assess their effectiveness in the regional model CHIMERE. We perform a 3D comparison of model outputs with each other and with a simulation devoid of LNOx. Model outputs are also compared with in situ measurements and satellite data. Furthermore, validating and evaluating these lightning parameterizations across different models (global and mesoscale) are crucial for fully assessing their robustness and applicability, underscoring the significance of this study. Additionally, a thorough evaluation of simulated tropospheric O_3 is also essential to refine model accuracy and deepen our understanding in the role of LNOx in ~~regional air quality and~~ atmospheric composition.

Furthermore, lightning-generated NOx also influences the tropospheric hydroxyl radical (OH) budget, in addition to affecting O_3 concentrations ~~(Murray et al., 2013; Murray, 2016)~~(Murray et al., 2013; Murray, 2016; Mao et al., 2021). The OH radical is primarily formed due to photolysis of O_3 ($O(^1D)$) at a shorter wavelength ($\leq$330 nm) in the presence of water vapour and secondarily through the reaction between hydroperoxyl radical (HO_2) and NO (Lelieveld et al., 2016; Banerjee et al., 2014). As a highly reactive and short-lived oxidant, with a lifetime of just a few seconds, OH is essential to tropospheric chemistry (Lelieveld et al., 2016). However, ~~significant~~ substantial variability exists among global models, ~~which differ by as much as (~~with differences of up to $\pm$30% ~~)~~ in estimating the mean OH burden (Murray et al., 2021). OH further controls the lifetime of many important trace gases, such as methane (CH_4), carbon monoxide (CO) and non-methane ~~VOCs~~ volatile organic compounds (NMVOCs) (Akimoto and Tanimoto, 2022; Luhar et al., 2021). For example, increase in OH burden reduces the lifetime of CH_4 (Equation R1), a potent greenhouse gas and a major contributor to global warming (Naik et al., 2013; Banerjee et al., 2014; Murray et al., 2021). By improving the parameterization of LNOx in CHIMERE, this study strengthens our understanding of tropospheric chemistry and the dynamics of trace gases.

$$CH_4 + OH \rightarrow CH_3 + H_2O \quad \text{(R1)}$$

Hence the specific objectives of the study are, (i) to ~~assess~~ evaluate and improve the ~~lightning flash parameterization~~ modelling of lightning flashes, with the CHIMERE model using the ~~CTH~~ classical CTH and the upgraded ICEFLUX scheme; (ii) to evaluate the effect of LNOx emissions on tropospheric O_3 and trace gases; (iii) the influence on the OH burden and lifetime of CH_4 quantified against the chemical loss. The detailed methodology is provided in Section 2. An analytical evaluation of the simulated results have been carried out and presented in the following sections.

2 Method of study

2.1 CHIMERE model configuration and experimental set-up

In this study, simulations are carried out with the CHIMERE chemistry-transport model (version 2023r2; Menut et al., 2024) over the domain of ~~northern hemisphere~~ Northern Hemisphere (NH) expanded from 0°–90°N, at a horizontal resolution of 100×100 km^2. Here, meteorological fields are forced externally to CHIMERE with a 3-hourly forecast dataset from European Centre for Medium-Range Weather Forecasts (ECMWF)– Integrated Forecasting System (IFS) (https://www.ecmwf.int/en/forecasts/dataset last access: 16 May, 2024). Simulations are done in twenty vertical levels in σ-pressure coordinates ranging from surface ~~(998 hPa)~~ to 200 hPa ~~over~~ for a period of one year (January–December, 2018) with a spin-up time of 15 days. The MELCHIOR2 scheme is used for ~~chemical mechanisms~~the chemical mechanism. The CHIMERE model employs a 10-bin logarithmic sectional size distribution ranging from 0.01 to 40 μm. Fields of chemical concentration are calculated with a time-step of few minutes, using an adaptive time-step, to ensure that the Courant-Friedrichs-Lewy (CFL) stability criterion is satisfied (Menut et al., 2021). ~~The chemical speciation of aerosols includes elemental carbon (EC), primary organic aerosols (POAs), secondary organic aerosols (SOAs), nitrates, sulfates, ammonium, dust, sea salt, and primary mineral particulate matter (PPM).~~ Boundary and initial conditions are derived from ~~climatological simulations of the global chemistry-transport model Laboratoire de Météorologie Dynamique General Circulation Model coupled with Interaction with Chemistry and Aerosols (LMDz-INCA3) for gaseous and particulate species (Hauglustaine et al., 2014)~~Copernicus Atmosphere Monitoring Service (CAMS) reanalysis dataset of atmospheric compositions produced by ECMWF, consisting of three-dimensional time-consistent atmospheric composition fields, including aerosols and chemical species (Inness et al., 2019), and from GOCART for dust concentrations (Chin et al., 2002). Biogenic emissions are provided by a reduced online version of the Model of Emissions of Gases and Aerosols from Nature (MEGAN) model (version 2.10) (Guenther et al., 2012). Mineral dust and sea-salt emissions are calculated using the schemes of Alfaro and Gomes (2001) and Monahan (1986), respectively. Anthropogenic emissions in the model are incorporated from CAMS-global and fire emissions are taken from CAMS Global Fire Assimilation System (GFAS, https://atmosphere.copernicus.eu/global-fire-emissions, last access: 16 May, 2024) The formation of SOA is as described in Pun and Seigneur (2007) and Bessagnet et al. (2008). The aerosol dynamic processes, such as condensation, coagulation, wet and dry deposition, absorption, and scavenging, are incorporated into the model (Menut et al., 2021). The mixing state is considered as internal homogeneous aerosol mixing (Menut et al., 2013). The online calculations for radiation and photolysis are incorporated using the FastJX module (Wild et al., 2000; Mailler et al., 2016). The horizontal ~~transport is~~ and vertical transports are solved with the van Leer (1977) scheme~~and vertical using Després and Lagoutière (1999) scheme (Lachatre et al., 2020)~~

. Boundary layer height and vertical diffusion are calculated by the ~~parametrization~~ parameterization proposed by Troen and Mahrt (1986) and deep ~~convection~~ convective fluxes are estimated using the Tiedtke (1989) scheme. Gaseous and aerosol species undergo dry or wet deposition and fluxes are calculated using the Wesely (1989) and Zhang et al. (2001) parameterization schemes. With access to anthropogenic and biogenic emissions, CHIMERE simulates 3D concentration for a range of gaseous and size-resolved particulate species, based on the chosen chemical scheme.

Simulations carried out for this study are (i) not including LNOx emissions (experiment: noLNOx), (ii) including LNOx emissions estimated with parameterization based on cloud top height (CTH) ~~developed by Price and Rind (1992), applying a correction factor over the land grids~~ (experiment: ~~wLNOx) . Anthropogenic emissions in the model are incorporated from Copernicus Atmosphere Monitoring Service (CAMS) -global and fire emissions are from CAMS Global Fire Assimilation System (GFAS, , last access: 16 May, 2024~~LNOx-CTH) and (iii) LNOx emissions estimated with parameterization based on ice flux (experiment: LNOx-ICEFLUX).

2.2 ~~Estimation~~ Parameterization of ~~LNOx emissions~~lightning flash

~~The LNOx emission calculation is done as per the CTH scheme (Price and Rind, 1992).~~

2.2.1 Cloud top height-based parameterization (CTH)

Derived from the theories advanced by Vonnegut (1963) and Williams (1985), ~~Price and Rind~~ Price and Rind (1992) formulated the CTH parameterization, wherein the flash rate is contingent upon the cloud top height (H_{top}). The distinct relationships governing flash rates over land and ocean are delineated as follows:

$$\begin{aligned} F_l &= a \times H_{top}^{4.9} \\ F_o &= b \times H_{top}^{1.73} \end{aligned} \tag{1}$$

Here, a and b are constants (values are provided in Table 1), H~~represents the cloud-top~~ $_{top}$ represents the cloud top height above the ground level in km~~,~~. Cloud-top height (H_{top}) and bottom height (H_{bottom}) are estimated based on the convection scheme of the model for each time step. F denotes the total flash ~~frequency~~ rate in flash number min^{-1} 25 km^{-2}, with subscripts 'l' and 'o' indicating land and ocean, respectively (Menut et al., 2020a). The distinction between land and ocean is employed to incorporate the disparity in updraft velocity over these two surface types. For instances where the cloud depth ($H_{top} - H_{bottom}$) is less than 5 km, the flash ~~value~~ number is set to zero~~, a criterion based on the data range utilized in developing the relationship by Price and Rind (1992)~~. This threshold reflects the physical condition necessary for charge separation and buildup in a storm to generate lightning. It's noteworthy that ~~Price and Rind (1994)~~ Price and Rind (1994) formulated an equation to adapt the above equations to various model resolutions. The scaling factor (C) determined to accommodate the model grid cell size is outlined as follows:

Table 1. Values of constants in Equation 1

~~constants Price and Rind (1992) present study (experiment: wLNOx) a 3.44×10^{-5} 6.88×10^{-6} b 6.40×10^{-4} 6.40×10^{-4}~~

constants	Price and Rind (1992)	present study (experiment: LNOx-CTH)
a	3.44×10^{-5}	3.44×10^{-6}
b	6.40×10^{-4}	3.20×10^{-4}

$$C = 0.97241e^{0.048203 \times \Delta x \times \Delta y} \quad (2)$$

Here, the product of longitude and latitude resolution, denoted as Δx $\times$ Δy, is measured in degrees^2. This factor typically remains close to 0.97, and its impact on the results is ~~generally~~ minimal, especially when compared to the uncertainties ~~of other parameters, except at very coarse resolutions~~due to other parameters. These uncertainties are ~~typically~~ offset by adjustment factors, that align the model more closely ~~with~~ to observations (Gordillo-Vázquez et al., 2019). ~~For example, in the study by Finney et al. (2014), a scaling factor of 0.05 has been applied to match the estimated flash rate to the satellite-based observation. In our study, we observe~~ In preliminary simulations, we observed a highly overestimated flash rate~~compared to satellite measurements, over the land grids from a preliminary simulation~~, estimated based on the formulations by Price and Rind (1992)~~. In this regard it is also to be noted that, satellites are unable to capture all the flashes, therefore providing minimized values of flash rate (Erdmann et al., 2020; Zhang et al., 2023).~~ , compared to the measurements from Lightning Imaging Sensor on the International Space Station (ISS-LIS) for the year 2018, over the land grids, followed by the ocean grids. Considering the overestimation in the modelled flash rate~~and the uncertainty in satellite-based observations~~, we have applied ~~a factor of 1/5 to constant~~ factors 0.1 and 0.5, respectively to constants 'a' and 'b' in Equation 1 over the land and ocean grids, in experiment ~~wLNOx~~LNOx-CTH, to reconcile the modelled lightning flash rate to the satellite observations (Table 1).

For each grid-cell, the relative ~~percentage~~ fraction of sea (x_{sea}) is determined using the land-sea mask from the land use database (Menut et al., 2020a). The ~~flash frequency~~ total flash rate (F_{CTH}) is then calculated as follows:

$$F_{CTH} = \frac{C \times (x_{\text{sea}} \times F_o + (1 - x_{\text{sea}}) \times F_l)}{25} \quad (3)$$

2.2.2 Ice-flux-based parameterization (ICEFLUX)

The equations used to estimate the flash rates in ICEFLUX parameterization are as follows (Finney et al., 2014):

$$f_l = 6.58 \times 10^{-7} \phi_{ice}$$
$$f_o = 9.08 \times 10^{-8} \phi_{ice} \quad (4)$$

~~Here, F represents total flash rate as flash number mn^{-1} km^{-2}.~~ here, f_l and f_o represent the flash rate (flash number $m^{-2}_{cell} s^{-1}$) over the lands and ocean, respectively. ϕ_{ice} denotes the upward ice flux ($kg_{ice}\, m^{-2}_{cloud}\, s^{-1}$) at 440 hPa and is determined using the following equation:

$$\phi_{ice} = \frac{q \times \Phi_{mass}}{c} \quad (5)$$

In this context, q represents the specific cloud ice water content at 440 hPa ($kg_{ice}\, kg^{-1}_{air}$), Φ_{mass} denotes the updraft mass flux at 440 hPa ($kg_{air}\, m_{cell}{}^{-2}\, s^{-1}$), and c represents the fractional cloud cover at 440 hPa ($m^2_{cell}\, m^{-2}_{cloud}$). Instances where c is less than 0.01 $m^2_{cloud}\, m^{-2}_{cell}$, upward ice flux is set to zero. Additionally, if no convective cloud top is identified, the flash rate is also set to zero (Finney et al., 2016a). The total flash rate ($F_{ICEFLUX}$) is then calculated as follows:

$$F_{ICEFLUX} = x_{sea} \times f_o + (1 - x_{sea}) \times f_l \quad (6)$$

2.2.3 Distribution of CG and IC lightning flashes

The empirically derived formula used to determine the relative proportion of 'cloud to ground (CG)' flashes in a single thunderstorm is initially based on the ~~cloud ice~~ cold cloud depth (H_f, from 0°C to cloud top) (Price and Rind, 1993). In this study H_f ~~is estimated in km as,~~ (in km) is calculated with the temperature profile in the model, estimating the freezing temperature height or the freezing level. The modelled H_f therefore varies from 6.9 to 7.76 km. The freezing level (0°C temperature), estimated in model, varies from 1 to 4.9 km, being the highest at tropics and decreasing with higher latitudes. The flashes from freezing level to the cloud top height is considered as 'in cloud (IC)' flashes and that from freezing level to ground as CG flashes.

$$H_f = -6.64 \times 10^{-5} |L|^2 - 4.73 \times 10^{-3} |L| + 7.34$$

~~Here, L represents the latitude in degrees. Parameter~~ The mean ratio of IC to CG flash rates (β ~~is calculated as follows:~~

$$\beta = 0.021H_f^4 - 0.648H_f^3 + 7.49H_f^2 - 36.54H_f + 64.09$$

~~where~~= IC/CG) is estimated as 3.09 from model estimates. β, in this study, is estimated with the empirical equation (Equation 7) by Price and Rind (1993), which is frequently used in several modelling studies (Luhar et al., 2021; Gordillo-Vázquez et al., 2019) . The empirical relationship between β and the cold cloud depth (H_f) was developed by Price and Rind (1993) based on data collected for 139 individual thunderstorms over the western United States (US) during summer. Several studies support the fact that the parameterization Price and Rind (1993) successfully estimate the distribution of CG and IC flashes in global as well as in mesoscale models (Pickering et al., 1998; Fehr et al., 2004). Theoretically, β varies between 1 to 50 for H_f ~~varies~~ varying between 5.5 to 14 km to prevent unrealistic values. The value of β estimated in our study is comparable to that obtained in recent modelling studies (Luhar et al., 2021; Gordillo-Vázquez et al., 2019). Wu et al. (2023) estimates the values of β as 2.94–3.70 with a lightning nitrogen oxides (LNOx) emissions model using satellite-observed lightning optical energy. Further, experiments conducted with satellite- and ground-based observations over different parts of the world also produce a β value in the range of 2.64–2.94 ($\pm$1.1–1.3) over US (Boccippio et al., 2001), 3–4 over India and China (Ghosh et al., 2023; Ren et al., 2024) . β obtained in our study again shows consistency with the above mentioned results.

$$\beta = 0.021H_f^4 - 0.648H_f^3 + 7.49H_f^2 - 36.54H_f + 63.09 \quad (7)$$

The relative part of CG in the total (~~in cloud (IC)~~ IC + CG) is denoted by p (Equation 8). The estimated value of p from our study is 0.25, aligning with findings from recent research (Luhar et al., 2021).

$$p = \frac{1}{1+\beta} \quad (8)$$

~~Finally, with the flash frequency and the vertical distribution of CG and IC for each flash, the NO emission is estimated in molecules flash~~Hence, the β in our study is not predetermined but is calculated based on the cold cloud thickness (H_f), estimated with temperature profile in CHIMERE and agrees well with the values estimated theoretically and from other model-based studies.

2.3 Estimation of LNOx emissions

Lightning flash energy estimates span a broad range from 0.35 to 5 GJ based on length-specific discharge values to up to 6.7 GJ considering contributions to the global atmospheric electric circuit (Krider et al., 1968; Uman, 2001; Price et al., 1997a). The NOx production rate per unit discharge energy also exhibits substantial variation, ranging from 1.1×10^{16} to 50×10^{16}

molecules J^{-1} ~~(Equation 9; Price et al., 1997a).~~ in laboratory experiments (Schumann and Huntrieser, 2007), and 5–15 $\times$ 10^{16} molecules J^{-1} in theoretical models (Price et al., 1997a). In this study, we adopt flash energies of 3 GJ for CG flashes and 0.9 GJ for IC flashes, along with a NO production rate of 14.2 $\times$ 10^{16} molecules NO J^{-1} (Schumann and Huntrieser, 2007). Using these values, we calculate the NO production in moles per flash as described in Equation 9, yielding a mean value of 332 moles of NO per flash. This estimation considers CG flashes as 25% of the total lightning flashes.

$$\begin{aligned} P(\text{CG, NO}) &= 697.44\,\text{moles flash}^{-1}, \\ P(\text{IC, NO}) &= 199.27\,\text{moles flash}^{-1} \end{aligned} \tag{9}$$

~~The NO~~ Recent research indicates comparable NO production rates for CG and IC lightning flashes, with a mean of 70–700 moles NO per flash (Bucsela et al., 2019; Ott et al., 2010; Finney et al., 2016a; Luhar et al., 2021). Despite this, significant differences in NOx production between IC and CG flashes are well-documented through theoretical models and observational studies, emphasizing the challenges and variability in quantifying NOx production rates (Gordillo-Vázquez et al., 2019; Carey et al., 2016; Koshak . Global modelling efforts, such as those using National Aeronautics and Space Administration (NASA) Goddard Earth Observing System (GEOS)-5 and GEOS-Chem systems, combined with satellite and airborne observations, have reported lightning NO production rates of 260 moles per flash (Jourdain et al., 2010), 246 moles per flash (Liaskos et al., 2015), and a range of 346 (over tropics) to 665 (for mid-latitude region) moles per flash (Nault et al., 2017). Additionally, Miyazaki et al. (2014) derived a global average of 310 moles NO per flash by integrating lightning data from the Optical Transient Detector (OTD) and the Lightning Imaging Sensor (LIS) with atmospheric composition measurements in a global chemistry-transport model. Overall, the mean NO production varies across 2 to 3 orders of magnitude in moles NO per flash, as noted by Bucsela et al. (2019); Murray (, although a mean value of 250 moles NO per flash has been suggested by Schumann and Huntrieser (2007). The estimates derived in this study is close to the values estimated by Miyazaki et al. (2014); Luhar et al. (2021), consistent with prior findings, underscoring the complexity of accurately assessing lightning-induced NO production. The NO_2 emissions are assumed to be 10~~% of the NO emissions. However, CTH parameterization simplifies the vertical structure of the emissions, considering the emissions to be evenly distributed over an altitude range, i.e. , the CG flux from the surface to H_f and the IC value from H_f to the cloud top (Menut et al., 2020a).~~ % of the NO emissions.

2.4 ~~Lifetime~~ Estimation of CH_4 lifetime due to chemical loss

The loss in tropospheric methane (CH_4) is primarily (90%) due to oxidation by hydroxyl radicals (OH, ~~Equation~~ Reaction R1)(Ghosh et al., 2015). The estimation of tropospheric chemical loss rate of CH_4 is as follows (in molecules cm^{-3} s^{-1}) (Zhao et al., 2023):

$$\text{rate} = k(T)[\text{CH}_4][\text{OH}] \tag{10}$$

where, [CH_4] and [OH] are the concentrations of CH_4 and OH (in molecules cm^{-3}). [OH] is taken from simulation in CHIMERE from our study, whereas [CH_4] is from chemical boundary conditions. The reaction rate (k(T) in cm^3 $molecule^{-1}$ s^{-1}) is temperature (T) dependent (Burkholder et al., 2019) and is represented in (Menut et al., 2013),

$$k(T) = 2.3 \times 10^{-12} \exp\left(-\frac{1765}{T}\right) \tag{11}$$

The total tropospheric chemical loss of CH_4 (L in Tg yr^{-1}) is estimated as,

$$L_{CH_4} = \int_V k(T)[CH_4][OH]\, dV \tag{12}$$

dV is the differential volume element in the troposphere. The lifetime of CH_4 (τ_{CH_4} in year) is expressed as,

$$\tau_{CH_4} = \frac{B_{CH_4}}{L_{CH_4}} \tag{13}$$

Here, B_{CH_4} is the annual tropospheric burden (in Tg) of CH_4. Note that, all the calculations in our study are done for NH.

2.5 Observation data for evaluation

Flash rate for the year 2018 from Lightning Imaging Sensor (LIS) on the International Space Station (ISS) platform, is used for evaluating flash rate estimated with the model (http://ghrc.nsstc.nasa.gov/; last access: 5 July, 2024). ISS-LIS optically detects lightning flashes that occur within its field-of-view during both day and night with storm-scale (4 km × 4 km) horizontal resolution (Blakeslee et al., 2020) ~~.~~ and 2 ms of temporal resolution. After time corrections comparing with Geostationary Operational Environmental Satellite (GOES) 16 and 17 Geostationary Lightning Mappers (GLM-16/17) and ground-based observations, the timing accuracy of ISS-LIS ~~allows expansion of~~ is better than its native precision of 2 ms. The flash detection efficiency of ISS-LIS is around 60% with diurnal variability of 51%–75% (Blakeslee et al., 2020). Monthly averaged flash rates are obtained from combined climatology product of satellite observations from the Optical Transient Detector (OTD) and the ~~long-term global lightning climatology from space and extends the global record to higher latitudes (~~Lightning Imaging Sensor (LIS), launched with the MicroLab-1 satellite, for the period of May, 1995 to December, 2014 (http://ghrc.nsstc.nasa.gov/; last access: 21 November, 2024). The product utilized in this study is the High Resolution Monthly Climatology (HRMC), which offers 12 monthly values at a horizontal resolution of 0.5° × 0.5°. Details are provided in Cecil et al. (2014).

For evaluating the vertical profile of O_3, altitudinal data measured by ozone-sonde, launched on small balloons, are downloaded from the World Ozone and Ultraviolet Radiation Data Centre (WOUDC, https://woudc.org/data, last access: 5 July, 2024) for the year 2018. Ozone-sonde data from 122, 977 and 121 stations are collected, respectively, over the tropical (0°–30°N),

mid-latitudes (30° N–60° N) and polar region (60° N–90° N). We also have used vertical O_3 profile data from Southern Hemisphere ADditional OZonesondes (SHADOZ) ozone-sonde measurements (https://tropo.gsfc.nasa.gov/shadoz, last access: 21 November, 2024) at four tropical stations (Kuala Lampur: 3.14°N, 101.69°E; Hanoi: 21.02°N, 105.80°E; Costa Rica: 9.62°N, −84.25°E and Hilo: 19.72°N, −155.08°E) for the year 2018. Global distributions of tropospheric column of ozone (TCO) are derived from the Ozone Monitoring Instrument (OMI) and Microwave Limb Sounder (MLS) on board the Aura satellite (https://acd-ext.gsfc.nasa.gov/; last access: 5 July, 2024) for the year 2018. The monthly mean TCO data from OMI/MLS are derived by subtracting the stratospheric column of ozone (SCO) from the total column of ozone measured by the OMI sensor. This process utilizes the tropospheric ozone residual (TOR) algorithm along with stratospheric ozone profile information from the MLS sensor (Ziemke et al., 2006). The dataset covers the spatial range of ±5560° ~~). The flash rate data from ISS-LIS is re-gridded to the resolution of simulated fields before comparison.~~ with a spatial resolution of 1° × 1.25°, spanning the period from October 2004 to December 2020.

This study utilizes total tropospheric column NO_2 from daily global gridded (0.25° × 0.25°) NO_2 Product from OMI L3-level (https://data.gesdisc.earthdata.nasa.gov/; last access: 2 December, 2024) for the year 2018 (Levelt et al., 2018). OMI is an ultraviolet-visible (UV-Vis) spectrometer on the polar-orbiting NASA Aura satellite, launched on 15 July, 2004 (Lamsal et al., 2021) . The simulated O_3 and NO_2 mixing ratio is compared with ground-based observation data from OpenAQ ~~(https://openaq.org, last access: 5~~ (https://openaq.org; last access: 5 July, 2024; Hasenkopf et al., 2015), U.S. Environmental Protection Agency (EPA, https://www.epa.gov~~,~~ ; last access: 5 July, 2024), European Environment Agency (EEA, https://www.eea.europa.eu~~,~~ ; last access: 5 July, 2024), Environment and Climate Change Canada (ECCC) data catalogue (https://data-donnees.az.ec.gc.ca, last access: 5 July, 2024), Subsistema de Informacion de Calidad del Aire (SISAIRE, http://sisaire.ideam.gov.co~~, ~~; last access: 5 July, 2024) and China National Environmental Monitoring Centre ~~(CNEMC, https://quotsoft.net/air/, last access: 5 July, 2024; Dufour et al., 2021)~~ (CNEMC, https://quotsoft.net/air/; last access: 5 July, 2024; Dufour et al., 2021), collected over the study period. The total number of observation stations over the NH are mentioned in Table 6. The evaluation of simulated data is done with the statistical analyses estimating the mean absolute bias (MAB), ~~normalised~~ normalized mean error (NME), and root mean square error (RMSE), using the annual mean of O_3 and NO_2 mixing ratio. ~~For evaluating the vertical profile of O_3, altitudinal data measured by ozone sonde, launched on small balloons, are downloaded from the World Ozone and Ultraviolet Radiation Data Centre (WOUDC, , last access: 5 July, 2024). Ozone sonde data from 122, 977 and 121 stations are collected, respectively, over the tropical (0°–30°N), mid-latitudes (30° N–60° N) and polar region (60° N–90° N).~~

3 Results and Discussions

3.1 ~~Evaluation of lightning flash rate and NOx emissions from lightning~~

~~The spatial distribution of average flash rates during the period of May–August, is presented in Figures 1b from experiment wLNOx. wLNOx is the simulation with CTH scheme applying a correction factor of 1~~

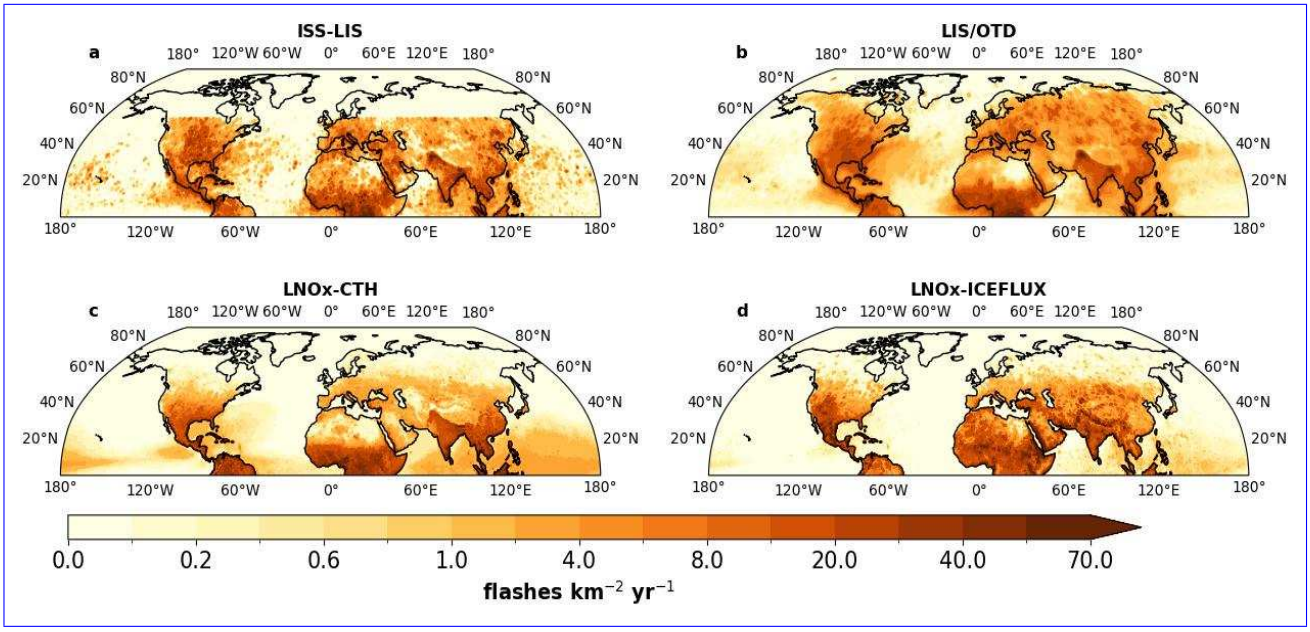

Figure 1. Spatial distribution of annual flash rates (flashes km^{-2} yr^{-1}) over NH based on (a–b) observations from (a) ISS-LIS satellite for the year 2018 (domain: 0–55°N) and (b) OTD/LIS climatology data (May, 1995 to December, 2014), (c–d) simulation experiments (c) LNOx-CTH and (d) LNOx-ICEFLUX.

3.1 Evaluation of modelled lightning flash rate

In this section we analyse the estimated lightning flash rates over the Northern Hemisphere (NH), from simulations conducted with CHIMERE model applying parameterization schemes based on cloud top height (experiment: LNOx-CTH) and ice flux (experiment: LNOx-ICEFLUX). The modelled flash rates from the two simulations are compared with observed flash rates from ISS-LIS (domain: ±55° latitudes) for the year 2018 and the combined climatology product of satellite observations from the OTD/~~5 over the land grids. Keeping the cruciality of representing the flash numbers in mind, specifically during~~ LIS for the period of ~~May–August, showing highest flash rates over NH (Christian and Petersen, 2005; Allen et al., 2010), the evaluation of the modelled flash rate for this period is done. The annual mean of flash rate from experiment wLNOx is also shown~~ May, 1995 to December, 2014. The spatial distribution of annual flash rates are presented in Figure 1~~d.~~. Please note that the flash rates over the land, estimated with ICEFLUX parameterization, are divided by 5 for each grid to match the ISS-LIS satellite observations.

As observed from our study, warm tropical regions (0°–30°N), especially central Africa, south America, India and south China are the regions with high lightning flash rate due to large convective activity, followed by the ~~mid-latitude region~~ mid-latitudes (30° N–60°N~~). The generation of LNOx has been reported to be significant in the tropics and mid-latitudes (Allen et al., 2010). The averaged~~ ; Figures 1c and 1d). South Asia, including India and south China, where significant flash rates are observed, are known to exhibit the greatest seasonal and interannual variation in lightning activities (Pawar et al., 2012a; Xu et al.,

. The annual flash rate ~~from wLNOx experiment~~ is observed as ~~0.8–1.5~~ 10–20 flashes km^{-2} ~~day~~yr^{-1} from both the experiments, over most of the tropical lands (~~Figure~~ Figures 1c and 1d)~~. South Asia, including India and south China, has been reported exhibiting the greatest seasonal and interannual variation in lightning activity (Pawar et al., 2012a; Xu et al., 2023). The spatial pattern of flash rate~~ , which is in agreement ~~with the~~ to the satellite observations from ISS-LIS ~~satellite-based observation~~ and LIS/OTD (Figures 1a and 1~~c)and other model-based studies (Finney et al., 2014, 2016a; Murray, 2016), but shows a pronounced bias over the tropical lands. The large bias over tropics is also observed in other model-based studies (Murray et al., 2012; Finne~~ . ~~After applying the correction factor over lands in experiment wLNOx, the bias is reduced to a factor ≈6 as averaged over~~ b). Over the mid-latitudes, flash rates are observed in the range 2–4 flashes km^{-2} yr^{-1}, while the polar regions (60° N–90°N) exhibit significantly lower values (0.1–0.2 flashes km^{-2} yr^{-1}) as indicated by the simulations as well as the satellite observations. Therefore, the tropical ~~lands for the period of May–August and ≈5 for annual mean of flash rate (Table 3). The bias over tropics is possibly due to the limitation of the CTH scheme by tropopause height which~~ and mid-latitude land regions dominate lightning activity. The spatial distribution of flash rates closely resembles the patterns observed in previous model-based studies using CTH and ICEFLUX schemes (Luhar et al., 2021; Gordillo-Vázquez et al., 2019; Finney et al., 2014, 2016a; Mu . However, patches of high flash rate observed in satellite data over central Canada, the United States, central European countries, and northern Russia are not reflected in the modelled flash rates from either experiment. Additionally, the elevated flash rates over central Asia are not captured in the LNOx-CTH simulation. Flash rates over land are significantly higher than the oceans due to intense convection over land regions (Albrecht et al., 2016). In oceanic regions, relatively higher flash rates (1–2 flashes km^{-2} yr^{-1}) are observed in the tropical regions, particularly over the Bay of Bengal and the Pacific Ocean, as simulated in LNOx-CTH experiment. Previous studies have reported inconsistencies in the equation for oceanic flashes developed by Price and Rind (1992) (Michalon et al., 1999; Boccippio, 2002; Luhar et al., 2021). However, our study demonstrates an improved flash rate distribution over tropical oceans, using the CTH scheme, compared to previous research (Luhar et al., 2021; Finney et al., 2016b). The magnitude of oceanic flash rates are significantly lower in simulations using the ICEFLUX scheme compared to the CTH scheme. ICEFLUX parameterization is based on charging theory, which is not enough to differentiate land and ocean flashes, e.g., more energetic less frequent flashes over oceans (Finney et al., 2014).

The spatial mean of annual flash rate over the NH tropics and NH tropical lands are comparable from two experiments, whereas, the flash rate from LNOx-CTH is lower than that from LNOx-ICEFLUX, by a factor of two at mid-latitudes (Table 2). These flash rates over tropics are 5–8 times higher than the mid-latitudes for NH and lands, as estimated from experiment with CTH. These factors are comparatively lower from experiment with ICEFLUX and from satellite observations, explaining the effectiveness of ICEFLUX scheme over CTH, in capturing flashes over the mid-latitudes. In CTH scheme, the estimated flash numbers are dependent on the cloud top height, which is limited by the tropopause height. The tropopause height is highest at equator and decreases away from the equator ~~(Finney et al., 2014). Uncertainty in flash rate datafrom ISS-LIS is also considerable in this context. The patches of high flash rate over the central region of Canada, United states of America (USA) and north-eastern region of China are found missing in~~ (refer to Table S1 in supplementary material presenting the tropopause and cloud top height). This restricts the cloud development to lower altitudes, resulting in a significant reduction in flash rates at higher latitudes (Finney et al., 2014). Spatially mean annual flash rates over tropical lands from both the experiments are

Table 2. Mean annual flash rate over NH, lands and ocean in NH for three latitude bands

Name of the experiments	mean flash rates (flashes km^{-2} yr^{-1}) 0°–30°N	30°–60°N	60°–90°N
NH			
LNOx-CTH	4.69	0.86	0.18
LNOx-ICEFLUX	4.55	1.54	0.36
Land in NH			
LNOx-CTH	10.95	1.46	0.55
LNOx-ICEFLUX	12.45	3.92	1.1
Ocean in NH			
LNOx-CTH	0.75	0.2	0.0003
LNOx-ICEFLUX	0.37	0.1	0.0002

Table 3. Statistical analysis of spatially varying annual flash rates from model comparing with ISS-LIS (OTD/LIS) satellite observations over NH, land and ocean in NH for three latitude bands. Latitudinal coverage for the ISS-LIS data is 0°–55°N. Statistical scores for comparison of simulated flash rates with OTD/LIS observations are provided in the parenthesis.

Name of the experiments	r$^{\perp}$ 0°–30°N	30°–60°N	60°–90°N	RMSE (flashes km^{-2} yr^{-1})$^{\perp}$ 0°–30°N	30°–60°N	60°–90°N	NME (%)$^{\perp}$ 0°–30°N	30°–60°N	60°–90°N
	NH								
LNOx-CTH	0.59 (0.73)	0.53 (0.66)	(0.5)	8.21 (6.64)	4.20 (4.06)	(1.15)	93.54 (65.28)	80.37 (76.15)	(96.77)
LNOx-ICEFLUX	0.31 (0.41)	0.28 (0.36)	(0.26)	12.23 (11.35)	5.70 (5.50)	(1.15)	119 (97.65)	108.11 (90.67)	(96.92)
	Land in NH								
LNOx-CTH	0.68 (0.82)	0.64 (0.63)	(0.3)	11.65 (9.52)	4.28 (5.15)	(3.22)	61.41 (37.68)	75.48 (74.34)	(96.88)
LNOx-ICEFLUX	0.15 (0.21)	0.27 (0.34)	(0.12)	21.50 (21.33)	9.34 (8.77)	(3.23)	110.65 (92.57)	154.87 (93.60)	(97.10)
	Ocean in NH								
LNOx-CTH	0.06 (−0.28)	0.15 (0.63)	(−0.1)	0.94 (0.61)	0.41 (0.35)	(0.10)	132.10 (87.88)	101.65 (94.26)	(100)
LNOx-ICEFLUX	0.06 (0.17)	0.14 (0.15)	(−0.1)	0.94 (0.69)	0.42 (0.37)	(0.10)	99.88 (98.88)	100 (99.88)	(100)

$^{\perp}$Correlation coefficient (r), RMSE and NME are estimated comparing simulated flash rates and ISS-LIS (OTD/LIS) satellite observations for the spatially varying annual mean flash rates.

close enough to the satellite measurements at tropics over NH and lands, while at mid-latitudes, only a good resemblance is observed for that from LNOx-ICEFLUX. On the other hand, the simulation with CTH scheme estimates the flash rates over tropical ocean as almost twice of that estimated using the ICEFLUX scheme, unlike that showed in previous studies (Finney et al., 2016b). We compare the spatially varying simulated annual flash rates with satellite observations (ISS-LIS and OTD/LIS) and the corresponding statistical metrics are presented in Table 3. Correlation coefficients for spatially varying flash rates show comparatively stronger correlations over the tropics and mid-latitudes of the NH and land regions, between that from LNOx-CTH and satellite data, compared to LNOx-ICEFLUX, being consistent with the findings by Clark et al. (2017). The flash rates from LNOx-CTH exhibit significantly higher correlations, particularly when evaluated against OTD/LIS data. Analysis of RMSE and NME also indicates lower errors for LNOx-CTH over these regions in comparison to that observed for LNOx-ICEFLUX, indicating the spatial variations of flashes from the first experiment align well with the satellite data.

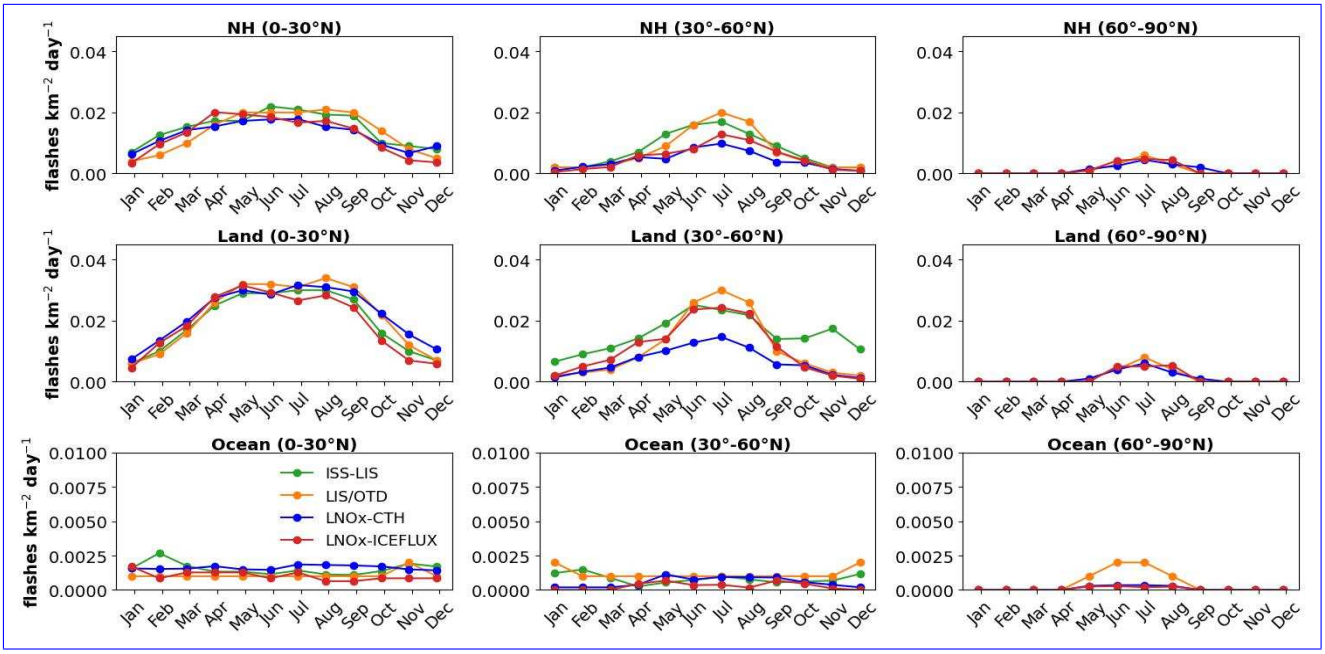

Figure 2. Comparison of monthly mean flash rates (flashes km^{-2} day^{-1}) from simulations (LNOx-CTH and LNOx-ICEFLUX) with ISS-LIS satellite observations for the year 2018 (domain: 0–55°N) and OTD/LIS monthly climatology (May, 1995 to December, 2014), over NH, land and ocean in NH for the three latitude bands. Please note that the Y-axis in the plots for oceans is presented on a different scale.

The worst performance is observed in the polar lands compared to the other two latitude bands, and also over oceanic region from both the experiments, characterized by weak correlations and higher errors. Hence, both schemes struggle to accurately simulate flash rates over oceans and high latitude lands. However, since lightning activity is minimal in these regions, the impact of this limitation is relatively minor. These results also highlight the ongoing challenges of accurately representing convection and capturing lightning flashes over the oceans. In summary, the statistical analysis points out the effectiveness of the ~~modelled flash rate (Figures 1b and 1d)~~ LNOx-CTH scheme in reproducing the spatially varying lightning flash rates reasonably well, particularly at tropics over NH and lands. However, both parameterizations exhibit limitations in the polar regions and over oceans, indicating scopes for further improvement in the parameterizations. Despite its lower overall performance in capturing spatial variation of flashes, LNOx-ICEFLUX shows lower bias in magnitude over mid-latitudinal land regions, suggesting the potential for refinement.

Figure 2 compares the monthly averaged lightning flash rates across different latitude bands in the NH, over land and ocean regions. The figure incorporates satellite observations (ISS-LIS and LIS/OTD) and results from two simulation experiments (LNOx-CTH and LNOx-ICEFLUX). Flash rates from the LNOx-CTH experiment show a clear seasonal cycle, with peaks occurring in May–August over NH and lands. During the winter months (November–January), flash rates drop significantly, being 5–7 times lower than the summer (May–August) peak values. The seasonal variation observed in the LNOx-ICEFLUX experiment and satellite observations closely align with this trend. Over land, both observations and simulations indicate high

Table 4. Statistical analysis of monthly mean flash rates from model comparing with ISS-LIS (OTD/LIS) satellite observations over NH, land and ocean in NH for three latitude bands. Statistical scores for comparison of simulated flash rates with OTD/LIS observations are provided in the parenthesis.

Name of the experiments	r‡ 0°–30°N	r‡ 30°–60°N	r‡ 60°–90°N	NME (%)‡ 0°–30°N	NME (%)‡ 30°–60°N	NME (%)‡ 60°–90°N
			NH			
LNOx-CTH	0.86 (0.84)	0.83 (0.94)	(0.97)	17.4 (24.5)	44.3 (43.1)	(34.6)
LNOx-ICEFLUX	0.92 (0.85)	0.89 (0.92)	(0.81)	24.8 (22.4)	33.6 (33.5)	(29.2)
			Land in NH			
LNOx-CTH	0.92 (0.98)	0.87 (0.97)	(0.97)	16 (11.3)	56.7 (41.1)	(23.5)
LNOx-ICEFLUX	0.92 (0.93)	0.85 (0.96)	(0.85)	23.4 (16.9)	31.5 (20.6)	(37.6)
			Ocean in NH			
LNOx-CTH	−0.1 (−0.28)	−0.48 (−0.49)	(0.87)	27.5 (57.3)	57.2 (53.7)	(78.3)
LNOx-ICEFLUX	0.04 (−0.17)	−0.74 (−0.49)	(0.88)	34.5 (32.9)	76.2 (76.5)	(83.8)

‡correlation coefficient (r) and NME estimated comparing simulated monthly mean flash rates and the same from ISS-LIS (OTD/LIS) satellite observations. ~~The simulated flash rate over the mid-latitude lands~~

Table 5. Estimated flash frequencies and LNOx emissions from simulations over NH. Flash frequencies in parenthesis are estimated for the domain 0–55°N, comparable to the ISS-LIS satellite data (23.6 flash s^{-1}). The flash frequencies from OTD/LIS climatology data are 26.4 and 25.3 flash s^{-1} over NH and for the domain 0–55°N.

Name of experiments	flash frequency (flash s^{-1})	total LNOx emissions (Tg N yr^{-1})	correction factor
LNOx-CTH	20.7 (20.64)	2.8	none
LNOx-ICEFLUX	21.6 (21.53)	3.1	5

flash rates, particularly in the tropics, followed by mid-latitudes for all the months. Peak lightning activity over lands occurs during late spring and early summer (May–August), corresponding to enhanced convective activity (Holle et al., 2016; Ghosh et al., 2023). In contrast, flash rates over oceans are consistently lower over all latitude bands. The tropical ocean shows an uniform flash rates throughout the year, without any prominent seasonality. The delay in the seasonal peak of flash rates over NH with CTH, and particularly with ICEFLUX, as noted by Finney et al. (2014), is not seen in our simulations. Therefore, using near-real-time, high spatially and temporally resolved meteorological data from ECMWF-IFS with continuous updates and improved configuration for advection in CHIMERE, we achieve an improved seasonal distribution that match well the satellite measurements.

The modeled monthly averaged flash rates from the simulations exhibit a strong positive correlation with satellite observations (ISS-LIS and OTD/LIS), with correlation coefficients ranging from 0.85 to 0.97 (Table 4). This agreement is consistent across all latitude bands over the NH, land regions, and the polar ocean region from both the experiments (LNOx-CTH and ~~ocean is relatively well-matched with~~ LNOx-ICEFLUX). These findings indicate that the simulations successfully capture the seasonal variability of flash rates. In contrast, a weaker negative correlation is observed over tropical and mid-latitudinal

oceans, indicating an inverse relationship between simulated and observed seasonality in flash rates in these regions. When comparing the simulated monthly flash rates with satellite observations, the results from LNOx-CTH align more closely with satellite observations at tropics than the mid-latitudes, as evidenced by lower NME at tropics over NH, land and ocean regions. Notably, the simulation LNOx-ICEFLUX exhibits a better performance at mid-latitudes than the LNOx-CTH, over NH and land regions, specially while compared with OTD/LIS measurements. Further, advancement in the seasonal representation of oceanic convection processes is essential for improving the simulation of flash rates over oceans.

The annual flash frequencies over the NH is estimated as 20.7 and 21.6 flashes s^{-1}, respectively from the LNOx-CTH and LNOx-ICEFLUX experiments (Table 5). These values are consistent with the satellite observations (23.6 and 26.4 flashes s^{-1}, respectively from ISS-LIS ~~observations, however shows an overestimation by factors 3–5.75 over the tropical oceans (Table 3). Nevertheless, controversies still remain on estimating lightning flashes over ocean and inconsistancies are found in the equation for ocean, developed by Price and Rind (1992) (Michalon et al., 1999; Boccippio, 2002; Luhar et al., 2021). The average flash rate during the period of May–August, is found to be twice the annual mean of flash rate from ISS-LIS-based observations , while it is higher by a small fraction (~~and OTD/LIS observation over NH) as well as to that obtained in recent model-based studies over NH (Luhar et al., 2021). While no scaling factor is applied in the simulated flash rates from LNOx-CTH, the flash frequency from LNOx-ICEFLUX is divided by a factor 5 ~~%–30%) in comparison to the annual mean rate from our study (experiment wLNOx~~to reconcile with the satellite-observed frequency. Accordingly, the evaluation of the results from LNOx-ICEFLUX has been conducted using flash rates adjusted by this factor. For instance, a recent study by Finney et al. (2016a) utilizing the UK Chemistry and Aerosol (UKCA) model determined that the global flash rate scaling factors required for the UKCA model are 1.44 and 1.12 for the CTH and ICEFLUX lightning parameterizations, respectively. Another study by Gordillo-Vázquez et al. (2019) produce scaling factors 2.05 and 4, respectively for the CTH and ICEFLUX lightning schemes in Community Atmosphere Model (CAM5). The ~~seasonality is however not well captured in the simulation, causing an overall high flash rate.~~

factors may vary up to 2–3 orders of magnitude to match observations, based on the lightning parameterization used and the results obtained (Tost et al., 2007; Finney et al., 2014).

In CTH parameterization, the assumption of minimum required cloud depth of 5 km, may introduce uncertainty in estimating lightning flashes, as it inherently assumes that every convective cloud with depth of 5 km corresponds to a thunderstorm (Luhar et al., 2021). It would be worthwhile to investigate the sensitivity of the modeled flash rates to the minimum cloud depth by varying this arbitrary threshold, either increasing or decreasing it. Similarly, the estimated flash numbers are very much sensitive to the choice of pressure levels for calculating ice flux in the ICEFLUX parameterization (Finney et al., 2014) . For example, it performs better at lower pressure levels (e.g., 340 and 440 hPa) but shows diminished correlations at higher pressure levels (e.g., 540 hPa). This sensitivity complicates its application across different regions and scales. Uncertainty also arises from the input meteorological data, model configuration and the detection efficiency of satellite measurements is also a significant factor when comparing the modeled flashes with satellite observations (Blakeslee et al., 2020; Erdmann et al., 2020; Zhang et al. .

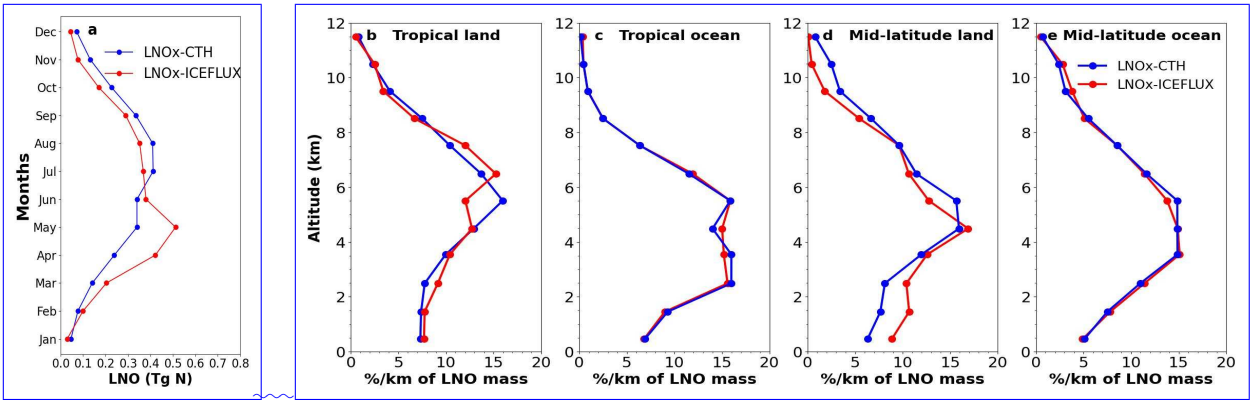

Figure 3. ~~Spatial distribution of flash rate (a–b~~a) ~~averaged over the period of May–August,~~ Monthly LNOx emissions in Tg N from simulations LNOx-CTH and LNOx-ICEFLUX. (~~ab–~~e) ~~ISS-LIS satellite-based observations~~ Vertical distribution of percentage of annual LNOx mass per kilometer from simulations LNOx-CTH and LNOx-ICEFLUX averaged over (b) ~~experiment wLNOx;~~ tropical land, (~~c–d~~c) ~~averaged over the year~~tropical ocean, ~~from~~ (~~c~~d) ~~ISS-LIS satellite-based observations~~ mid-latitudinal land and (~~d~~e) ~~experiment wLNOx~~mid-latitudinal ocean.

3.2 NOx emissions from lightning

~~Comparison of modelled flash rate to ISS-LIS based observation over land and ocean0°–30° N 30° N–55° N 0°–30° N 30° N–55° N Land 6.10 2.03 5.23 1.64 Ocean 3.17 0.52 5.75 0.46~~

The production of LNOx emissions depends on the average flash frequency (in flashes s^{-1}) and the NOx production efficiency per flash, which represents the rate of NOx emissions per flash (Schumann and Huntrieser, 2007; Gordillo-Vázquez et al., 2019; L. In this study, the mean LNOx emission per flash is estimated as 332 mol. The estimated annual NO ~~emission from lightning in experiment wLNOx is 8.82~~ emissions from lightning are 2.8 Tg N yr^{-1} and 3.1 Tg N yr^{-1} over the NH, respectively from LNOx-CTH and LNOx-ICEFLUX simulations (Table 5). Notably, LNOx emission from LNOx-ICEFLUX is 7.5% higher than that from LNOx-CTH. Recent studies estimate ~~that global NO emissions from lightning (LNO) to be typically within the range of~~ global LNOx emissions typically range from 2 to 8 Tg N yr^{-1} (Schumann and Huntrieser, 2007; Finney et al., 2016b; Nault et al., 2017), ~~but may vary within a wide range~~ with variations reaching up to 25 Tg N yr^{-1} ~~(Price et al., 1997a, b). The study by Luhar et al. (2021) shows that, the LNO emissionsare almost equally contributed from both northern and southern hemispheres, while estimated in a global chemistry-climate model, applying the CTH scheme. Considering this ,~~ in extreme scenarios (Price et al., 1997a, b). Price et al. (1997b) suggested that, the global annual LNOx emissions cannot be less than 5 Tg N or exceed 25 Tg N. The LNOx emissions from our study align well with the estimates by Luhar et al. (2021), which ranged from 2.39 to 3.41 Tg N yr^{-1} over the NH when using CTH and a new parameterization by Luhar et al. (2021). A recent study shows that the ~~LNO emission estimated in our studylies within the range of global LNO emissions as mentioned above. CTH scheme though oversimplifies the complex interactions and distributions of charge that contribute to lightning production (Price and Rind, 1992; Finney et al., 2014). It does not account for~~ estimated global LNOx emissions, with CTH scheme and the new parameterization by Luhar et al. (2021), are respectively 5.66 and 5.58 Tg N yr^{-1} in the model

EMAC (Pérez-Invernón et al., 2024). These estimates are respectively, 17% higher and 15% lower than that estimated by Luhar et al. (2021) with the same parameterizations, showing the LNOx emissions are highly sensitive to the model configurations. The monthly variation in LNOx emissions, in our study, from the two simulations is shown in Figure 3a. The results indicate that peak emissions occur in July–August, followed by May–June and September, in the LNOx-CTH experiment. The emissions from the LNOx-ICEFLUX experiment peak in May, followed by the remaining summer months (April, June–August). Approximately 60%–70% of the total annual LNOx emissions are contributed during late spring and summer (April–August), when lightning activity is at its highest.

The Figures 3b–3e represent the vertical distribution of LNOx emissions as percentage of LNOx mass per km. The distribution shows the maximum of LNOx mass lies between the altitude range of 4–7 km at all regimes from both the simulations, showing the typical 'backward C-shape' (Ott et al., 2010). 60–65% of LNOx mass is injected at this altitude range. Here it is to be mentioned that annually 1.85 and 1.9 Tg N LNOx are being generated over tropical land as obtained from LNOx-CTH and LNOx-ICEFLUX simulations, respectively, being almost 63%–66% of total annual LNOx over NH. The amounts are 0.55 (0.76), 0.15 (0.09) and 0.07 (0.03) Tg N for mid-latitudinal land, tropical ocean and mid-latitudinal ocean respectively, from LNOx-CTH (LNOx-ICEFLUX) simulation. Therefore, the mid-tropospheric region (4–8 km) contributes the maximum of the LNOx mass, specially over the tropical land region. The vertical profiles available from previous studies reveal a similar shape of all the profiles but contributing maximum at upper tropospheric region (within 2–4 km of the tropopause) rather than mid-troposphere. However, the study by Pickering et al. (1998) represents a high emission near surface due to strong downdraft, where the distribution is low and almost uniform up to 5–6 km as observed from the studies by Ott et al. (2010); Luhar et al. (202 . Nevertheless, the profile over mid-latitude lands from our study matches well with that from the study by Ott et al. (2010), with a maximum at 5 km. In our study, 13%–19% of total LNOx mass is estimated from surface to up to 2 km over tropical and mid-latitude lands and tropical oceans. LNOx production is suggested to be proportional to atmospheric pressure by Goldenbaum and Dickerson (1993); Pickering et al. (1998). Notably, a simple vertical structure of the emissions is adopted in this study, considering the emissions to be evenly distributed over an altitude range. The vertical distribution of LNOx mass can be improved by replacing the simple distribution currently used, with the more detailed scheme developed by Pickering et al. (1998).

3.3 Vertical distribution of gases: effects of LNOx

3.3.1 Ozone

Numerous studies have demonstrated that LNOx emissions play a significant role in influencing the levels of ozone and other trace gases as a result of the oxidation of CO, CH_4 and volatile organic compounds (VOCs), particularly in the free troposphere (Luhar et al., 2021; Mao et al., 2021; Finney et al., 2016b; Liaskos et al., 2015). The changes in the annual mean of O_3 mixing ratio, due to the inclusion of LNOx in simulation LNOx-CTH, with respect to that from simulation noLNOx, averaged over four altitude bands (998–900, 900–750, 750–500 and 500–200 hPa) is presented in Figure 4. The changes in the same from experiment LNOx-ICEFLUX with respect to LNOx-CTH, are also produced in Figure 5. The highest increase in simulated O_3

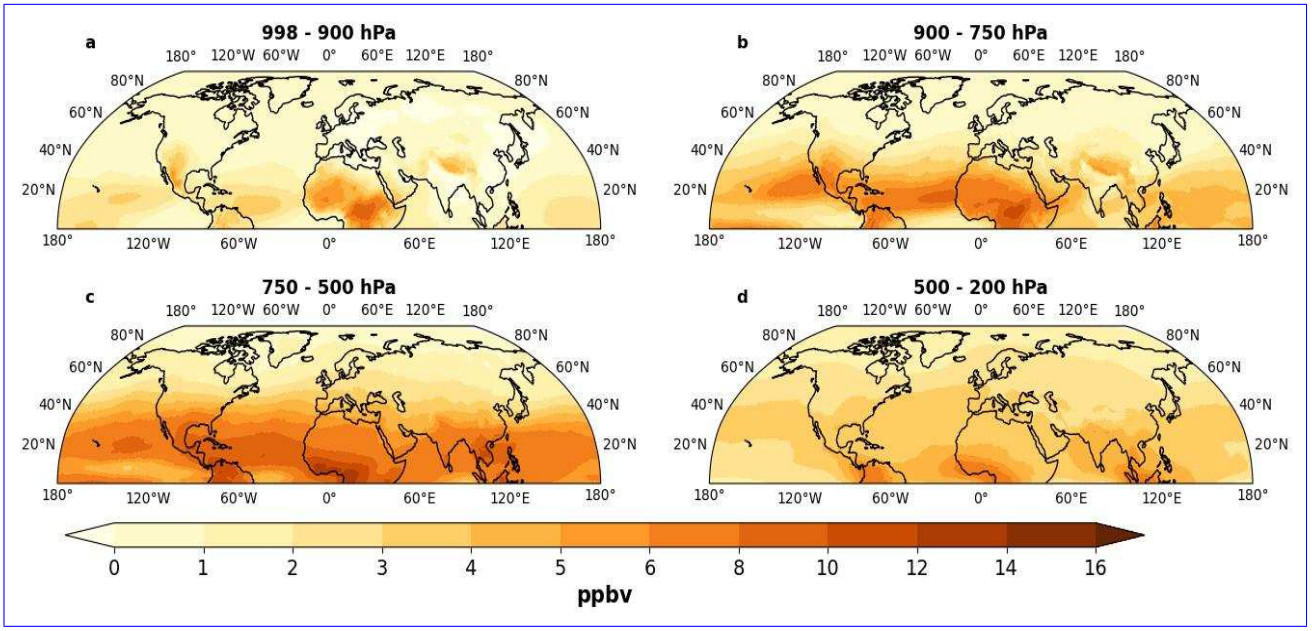

Figure 4. Changes in annual mean of O_3 mixing ratio from experiment LNOx-CTH w. r. t. noLNOx (ΔO_3) at the altitude bands of (a) 998–900 hPa, (b) 900–750 hPa, (c) 750–500 hPa and (d) 500–200 hPa; positive and negative values represent the increase and decrease in the O_3 mixing ratio, respectively.

is observed in the altitude band 750–500 hPa, specifically over the tropics, by 6–10 ppbv. 4–6 ppbv increase over the tropics is also observed at the altitude bands 900–750 hPa and 500–200 hPa (mid- to upper troposphere). The increase is maximum over the tropical region of America, central Africa, southern Asia and the Maritime continents in south-east Asia (Indonesia, Philippines and Malaysia). The above-mentioned regions with comparatively larger increase in O_3, identified for all the altitude bands, are observed as regions with the largest convection depth and LNOx emissions (Banerjee et al., 2014). A higher value by 2–4 ppbv in annual mean O_3 is also observed from LNOx-ICEFLUX, with respect to LNOx-CTH over the tropical region for the altitude band 750–500 hPa, followed by 900–750 hPa band (Figure 5). Even higher increase over the tropical region of America, central Africa and Tibetan Plateau is also found from LNOx-ICEFLUX. On the other side, the changes in O_3 mixing ratio are insignificant over mid-latitudes and polar regions from both the simulations with respect to noLNOx. The percentage changes in the annual mean of O_3 mixing ratio from LNOx-CTH with respect to noLNOx, averaged over selected latitude and altitude bands present an overall improvement in tropospheric O_3 (Table S2 in supplementary). O_3 levels are significantly elevated by 10%–19% in the mid and upper troposphere (750–200 hPa), where O_3 production occurs efficiently (Dahlmann et al., 2011). Tropical mid- and upper tropospheres are more crucial in O_3 production as most lightning discharges occur in these regions (Luhar et al., 2024; Bucsela et al., 2019; Murray, 2016). A moderate (3%–5%) to low (1%–2%) increase in mid and upper tropospheric O_3 is also observed over mid-latitudes followed by the polar region. Higher O_3 mixing ratios are observed in LNOx-ICEFLUX compared to LNOx-CTH in the mid to upper troposphere across all latitude bands, likely due to comparatively higher LNOx production from LNOx-ICEFLUX in these regions.

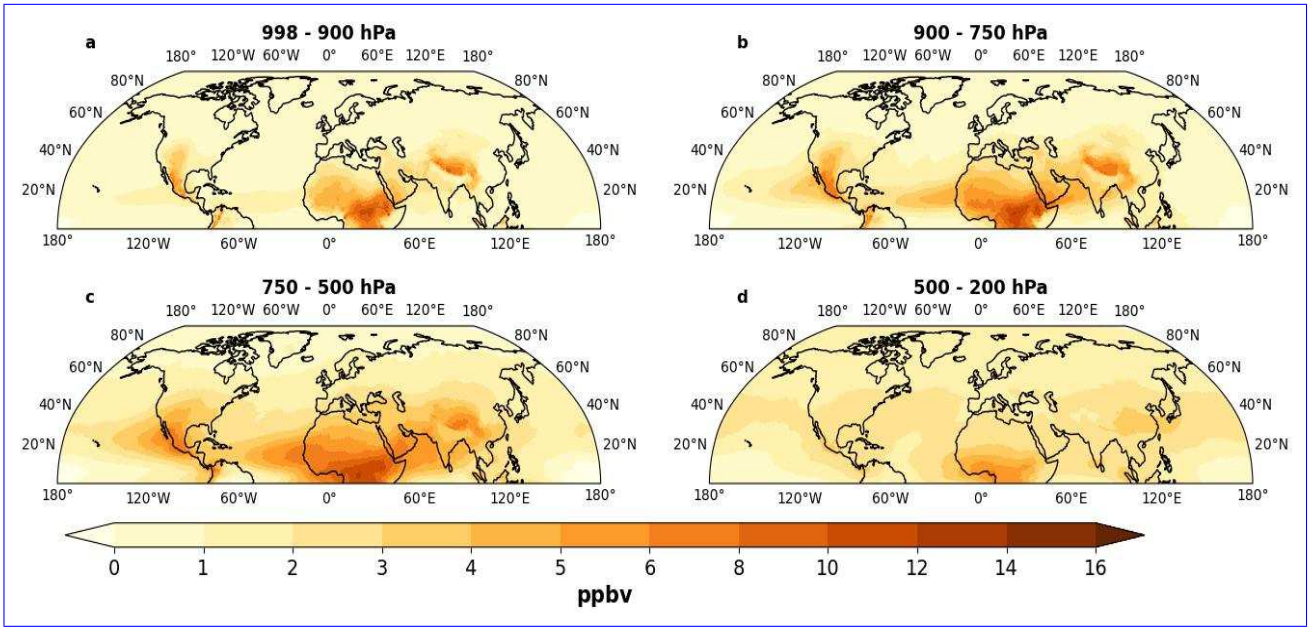

Figure 5. Changes in annual mean of O_3 mixing ratio from experiment LNOx-ICEFLUX w. r. t. LNOx-CTH at the altitude bands of (a) 998–900 hPa, (b) 900–750 hPa, (c) 750–500 hPa and (d) 500–200 hPa; positive and negative values represent the increase and decrease in the O_3 mixing ratio, respectively.

Figure 6 represents the vertical profile of annual mean O_3 mixing ratio from simulations and their comparison with the WOUDC ozone-sonde measurements, averaged for the stations over three latitude bands (0°–30° N, 30° N–60° N and 60° N–90° N). The upper tropospheric O_3 mixing ratio is moderately higher than that observed at surface at the tropics by 30%–60%, while it is 2–3 times higher over the mid-latitudes and polar region as observed from simulation LNOx-CTH (Table S2 in supplementary). The upper tropospheric O_3 over the polar region is also almost twice of that over the tropics (Table S2 in supplementary). Notably, the vertical profile from observations represents an increasing O_3 mixing ratio with altitude, whereas, those from simulations show an overestimated O_3 mixing ratio near surface which tend to decrease near the boundary layer in the tropics (Figure 6). The simulated O_3 is also observed to be higher near surface and show a continuous increasing pattern over mid-latitudes and polar regions. It is visible in Figure 6, that the simulated O_3 mixing ratio from the experiments with LNOx, represents the measured O_3 adequately well, specifically in the free troposphere over tropics, where a large underestimation is observed in simulated O_3 from noLNOx simulation. The absolute bias in simulated O_3 in the free troposphere, especially over the tropics, is reduced due to inclusion of LNOx in the model (Table S3 in supplementary). The bias is however lower for that from LNOx-CTH in comparison to LNOx-ICEFLUX. O_3 production efficiency due to LNOx is higher in the mid to upper troposphere, primarily because lower temperatures extend the lifetime of NOx, while enhanced photolysis rates further favour O_3 accumulation (Labrador et al., 2005). The high underestimation in the simulated O_3 mixing ratio in the altitude band 500–200 hPa, i.e., the upper troposphere and lower stratosphere, over mid-latitudes and polar regions still exists, even after

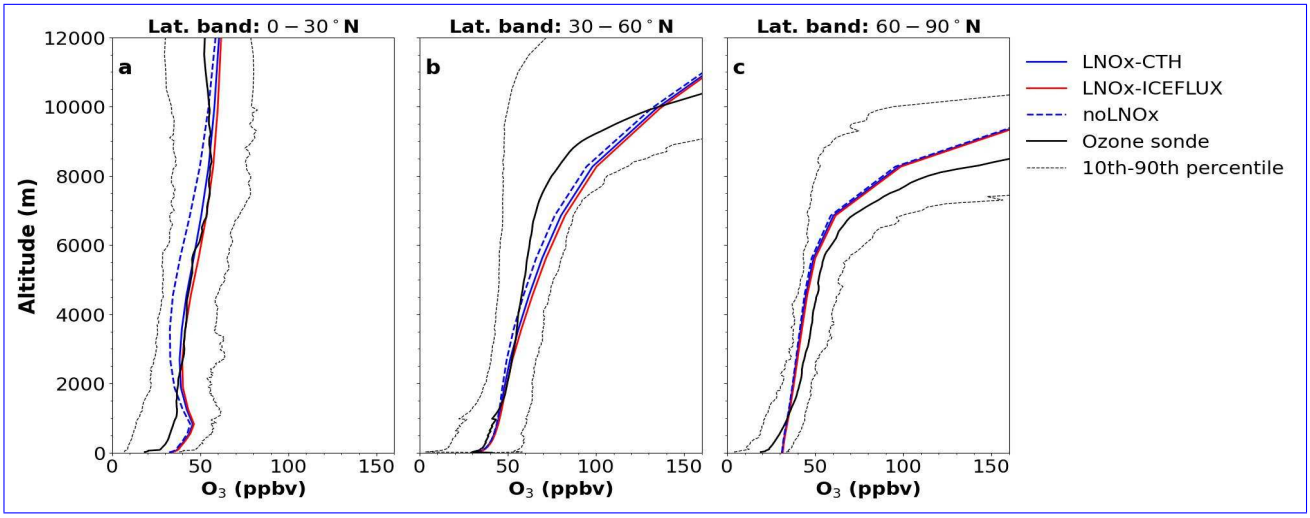

Figure 6. Vertical profile of annual mean of O_3 mixing ratio from noLNOx (blue dashed line), LNOx-CTH (blue solid line) and LNOx-ICEFLUX (red solid line) simulations and comparison with the WOUDC ozone-sonde measurements (black solid line), averaged for the stations over the latitude bands (a) 0°–30° N, (b) 30° N–60° N and (c) 60° N–90° N; the black dashed lines indicate the 10 and 90 percentiles of the WOUDC ozone-sonde measured values.

the inclusion of LNOx, however lower underestimation is observed for LNOx-ICEFLUX. The underestimation represents that improvement in the modelled stratosphere-troposphere exchange still requires a lot of refinement and further investigation.

We also compare the vertical profiles of simulated O_3 with that from SHADOZ ozone-sonde measured data at stations of Kuala Lampur, Hanoi, Costa Rica and Hilo, situated over the NH tropics. The plots are provided in supplementary material (Figure S1). Among the stations, at Kuala Lampur, the simulated O_3 profile from LNOx-ICEFLUX shows a good match with the observations at free troposphere, while the profile from LNOx-CTH aligns well with observations at Costa Rica. However the modelled O_3 profiles show under- and overestimation at most of the altitudes, respectively at Hanoi and Hilo, but overall replicate the observed altitudinal distribution quite well. The comparisons once again represents the effect of LNOx on O_3, specifically at the free troposphere.

The monthly comparison of simulated O_3 from the LNOx-CTH and LNOx-ICEFLUX experiments with WOUDC ozone-sonde measurements, is presented in Figure S2 in the supplementary material, across two altitude (750–500 hPa and 500–200 hPa) and three latitude bands. The monthly variation reveals the highest peaks during March and October in the tropics, with the lowest levels observed during June–July for both altitude bands. A similar variation is noted at mid-latitudes and in the polar regions for the 750–500 hPa altitude band, aligning well with the observed monthly trends. The simulated O_3 from both experiments closely matches the observed values at the tropics and mid-latitudes for both altitude bands, exhibiting a low bias of ±3–10 ppbv. However, an overestimation of simulated O_3 is apparent during January–April, particularly over the tropics. While there is a good agreement between simulated and observed O_3 over the polar region for the ~~complex microphysical processes, storm dynamics and presence of ice particles as well (Price and Rind, 1992), explaining the insufficiently reproduced seasonality in~~ 750–500 hPa altitude band, a significant underestimation of simulated O_3 is evident in the ~~flash rate in our study. The limitations~~

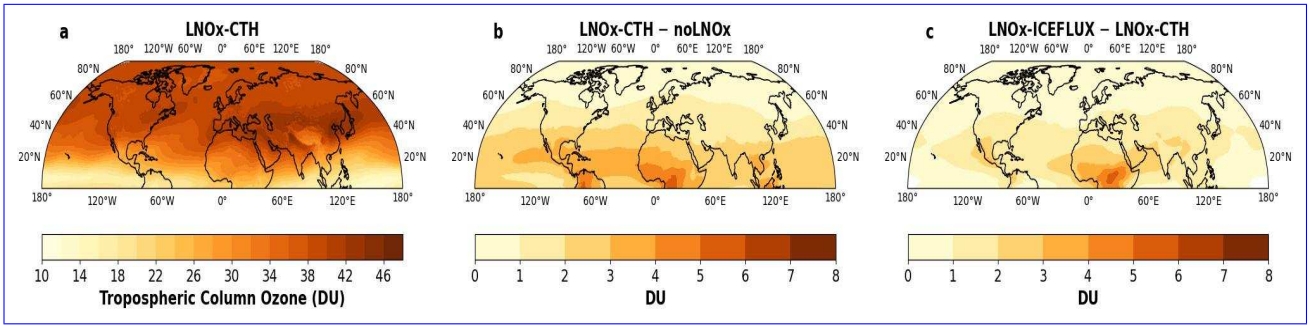

Figure 7. (a–c) Spatial distribution of (a) simulated tropospheric column ozone (TCO) in DU, over the NH from experiment LNOx-CTH, (b) changes in simulated TCO over NH from experiment LNOx-CTH w. r. t. noLNOx simulation, (c) differences in simulated TCO over NH from experiment LNOx-ICEFLUX w. r. t. LNOx-CTH; positive and negative values represent the increase and decrease, respectively.

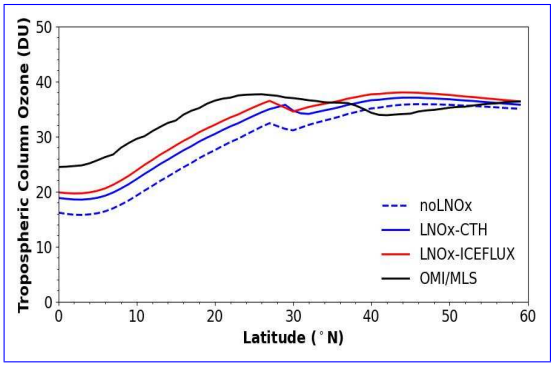

Figure 8. Zonal average of TCO from simulations over NH and their comparison with the same from OMI/MLS.

~~further motivate us to conduct a study in future, applying new schemes that include more parameters in order to represent the average and variability of flash numbers better~~500–200 hPa altitude band as discussed previously.

The spatial distribution of tropospheric column of ozone (TCO) from the LNOx-CTH simulation, along with the changes in TCO relative to the noLNOx and LNOx-ICEFLUX simulations, are shown in Figure 7. The TCO is observed to increase from the tropics toward higher latitudes, with the higher values occurring over the mid-latitudes (32–42 DU), particularly over Asian countries (40–44 DU; Figure 7a). The lower TCO values in the tropics are attributed to the model's top height being lower than the tropopause height in this region (refer to the Table S1 in supplementary material presenting the tropopause height). The TCO from the LNOx-CTH simulation is higher by 2-4 DU at tropics, than that from the noLNOx simulation, while the LNOx-ICEFLUX simulation produces even higher TCO values compared to LNOx-CTH, especially over the tropics (Figures 7b–7c). The tropospheric O_3 burdens, estimated from the simulation LNOx-CTH and LNOx-ICEFLUX, are respectively 176 (150) Tg and 182 (155) Tg, over the NH and over the domain of 0°–60°N (presented inside parenthesis). These burdens represent a 7%–11% increase relative to the noLNOx simulation (Table 8). Notably, the estimated O_3 burden in this study aligns closely with observations from OMI/MLS (159 Tg) for the domain of 0°–60°N. The spatial distribution of TCO from OMI/MLS is shown in Figure S3 in supplementary material. A comparison of the zonal mean TCO over 0°–60°N reveals good

agreement between the simulated TCO and OMI/MLS observations in the mid-latitudes (Figure 8). However, the simulations underestimate TCO in the tropics by 7%–26%, owing to the limited model top height, which excludes part of the troposphere above it. Despite this limitation, incorporating LNOx into the model leads to significant improvements in simulated TCO.

3.3.2 NO_2

Figure 9a represents the spatial distribution of NO_2 column density estimated from LNOx-CTH. 2–3 $\times$ 10^{15} molecules cm^{-2} NO_2 column densities are observed over the southern and eastern Asia (India and eastern China), north-west Europe and eastern part of USA. The spatial variation in NO_2 column matches well with that obtained from OMI observations (Figure S4 in supplementary material), highlighting elevated NO_2 column densities in countries with significant industrial activities (Cooper et al., 2022). However a decrease in NO_2 column density (0.2–0.6 $\times$ 10^{15} molecules cm^{-2}) is observed over the above mentioned continents due to inclusion of LNOx in model (Figure 9b). LNOx primarily produces NO, which rapidly oxidizes to form NO_2 in the presence of O_3, initially increasing the NO_2 level. However, rapid photolysis of NO_2 and its reaction with OH accelerate its conversion to HNO_3, leading to subsequent removal and a net decrease in NO_2 concentration (Labrador et al., 2005; Schumann and Huntrieser, 2007). Again, small increases of 0.1–0.2 $\times$ 10^{15} molecules cm^{-2} are observed over Africa, South America, and tropical oceans. Notably, NO_2 column densities from LNOx-ICEFLUX are higher by 1.0–1.2 $\times$ 10^{15} molecules cm^{-2} compared to LNOx-CTH over southern Asia, central Africa, and parts of the United States (Figure 9c).

The zonally averaged NO_2 column distribution (Figure 10) reveals elevated column densities over the tropics, especially between 20°–30°N, and the mid-latitudes, even in the absence of LNOx emissions. The zonal averages range from 0.35–1.75 $\times$ 10^{15} molecules cm^{-2} in these regions, which is nearly double the values observed at higher latitudes (60°–90°N). The peak at 20°–30°N is, however not observed in satellite observations. The higher uncertainty in tropospheric NO_2 columns retrieved from OMI observations is attributed to the complexity of tropospheric processes and the sensitivity of retrievals towards pollution levels (Bucsela et al., 2013). The simulations also identify a secondary maximum in NO_2 column density at 35°–45°N, which aligns with satellite observations over the mid-latitudes. At higher latitudes, where the magnitudes are comparatively lower, the simulated NO_2 column density matches well with satellite-based observations. Overall, the zonally averaged NO_2 column densities from the simulations closely replicate satellite observations, except for a pronounced peak at 20°–30°N from simulated NO_2. The tropospheric burden of NO_2 is 146 Gg from LNOx-CTH, being comparable to that from noLNOx and 11% lower than that estimated from OMI (Table 8). The burden estimated from LNOx-ICEFLUX is 18% and 5% higher than the LNOx-CTH and OMI, respectively.

3.4 ~~Impact of lightning on surface-level O_3 and precursor gases~~

3.4 Impacts of LNOx on surface-level O_3 and NO_2

~~The underestimation in emissions is a major source of uncertainty in simulated fields, highlighting the need for a more accurate representation of emissions in models. LNOx is one of such uncertain emissions, that has been incorporated into models over~~

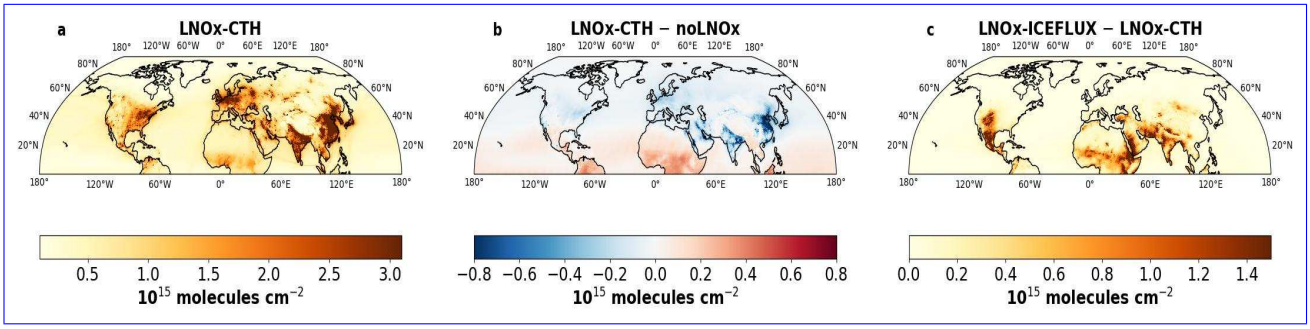

Figure 9. (a–c) Spatial distribution of (a) simulated NO_2 column in 10^{15} × molecules cm^{-2}, over the NH from experiment LNOx-CTH, (b) changes in simulated NO_2 column over NH from experiment LNOx-CTH w. r. t. noLNOx simulation, (c) differences in simulated NO_2 column over NH from experiment LNOx-ICEFLUX w. r. t. LNOx-CTH; positive and negative values represent the increase and decrease, respectively.

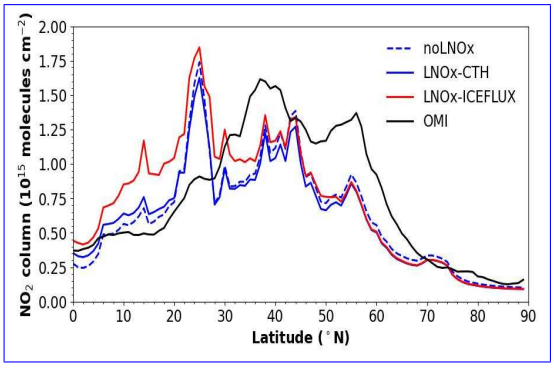

Figure 10. Zonal average of NO_2 column from simulations over NH and their comparison with the same from OMI.

~~the past few decades (Allen et al., 2010; Banerjee et al., 2014; Finney et al., 2016a; Kang et al., 2019, 2020). In this study , we have conducted a simulation with LNOx emissions in a chemistry transport model CHIMERE and the effect~~ The effect of LNOx on surface level O_3 and ~~nitrogen dioxide (~~NO_2 ~~)~~ over NH is analysed in this section.

~~(a, d) Spatial distribution of annual mean mixing ratio in ppbv at the surface over NH from experiment wLNOx for (a) O_3, (d) NO_2; (b, e) changes in mixing ratio at the surface due to inclusion of LNOx emissions for (b) O_3, (e) NO_2, positive and negative values show an increase and decrease, respectively; (c, f) absolute bias in simulated mixing ratio at surface at stations for (c) O_3, (f) NO_2, positive and negative values of absolute bias represent that modelled O_3 and NO_2 are higher and lower than the measurements, respectively.~~

The spatial distribution of the annual mean of O_3 mixing ratio and NO_2 at the surface from experiment ~~wLNOx~~ LNOx-CTH and changes in the mixing ratio due to inclusion of LNOx (ΔO_3 and ΔNO_2), are presented in Figures 11a, 11d and 11b, 11e, respectively. Other than natural sources (e.g., lightning, soil-NOx emissions), emissions from fossil fuel combustion for transportation, industrial activities, energy generation and biomass burning also have a profound influence on tropospheric O_3 and NO_2 concentrations (Lelieveld and Dentener, 2000; van der A et al., 2008; Butler et al., 2020). In our study, the O_3 mixing

ratio at the surface ~~represents a spatial variation~~ varies spatially with higher values ranging between ~~40–60~~ 35–45 ppbv over the ~~tropics and mid-latitudes up to 50~~latitude band of 10°–50°N, specifically over the lands, being almost 1.5–2 times of that observed over the rest ~~part of~~ of the NH. The NO_2 at the surface, is within a range of 0.5–2 ppbv over most parts of the NH showing higher magnitudes over USA, western Europe, India, eastern China and Japan (5–10 ppbv). To indicate the impact of LNOx emissions on changes in surface-level O_3 and NO_2, annual mean of mixing ratio obtained from experiment ~~wLNOx~~ LNOx–CTH is compared with respect to that from noLNOx. The positive and negative values of ΔO_3 and ΔNO_2 depict an increase and decrease, respectively, in surface mixing ratio (Figures 11b and 11e). The study shows an overall increase in surface O_3 by ~~2–5~~ 1–3 ppbv over most parts of the tropical lands and mid-latitudes up to 50°N (Figure 11b), while the increase is almost negligible over 50°–90°N (<1 ppbv). A comparatively larger increase by ~~5–10~~ 3–5 ppbv is observed over tropical parts of America and Africa and the Tibetan Plateau, but is particularly noteworthy (~~10–25~~ 5–10 ppbv) over the central part of Africa, which is a hotspot location with high lightning flash rate (~~Figure 1d~~Section 3.1). Unlike O_3, NO_2 exhibits both increase and decrease in mixing ratio at the surface as an effect of lightning (Figure 11e), but by a ~~very weak value~~ lesser magnitude (0.01–0.1 ppbv). While the increase is observed over ~~most of the tropical and mid-latitude lands~~South America, Africa, the Maritime Continent and south-east Asia, a decrease in NO_2 mixing ratio is also there ~~at high altitude Himalayan region at north of India, northern China,~~ over India, south-west Asia and ~~a few areas over Canada~~most of the continents north of 30°N. O_3 and NO_2, both exhibit a slight increase over the Atlantic ~~, Indian and Pacific Oceans~~ and Pacific oceans in the tropics. The magnitudes and spatial patterns of ΔO_3 and ΔNO_2 from our study bear a resemblance to those from recent studies (Murray, 2016; Li et al., 2022; Cheng et al., 2024). The impact on surface O_3 and NO_2 concentrations is a localized effect of thunderstorms, crucially influenced by the specific photochemical conditions in the area (Murray, 2016). An increase in surface O_3 levels due to LNOx suggests the NOx concentration to be below the titration threshold (Pawar et al., 2012b).

~~Figures 11c and 11f~~

The statistical analyses are also done comparing the simulated mixing ratios at surface to the observations and presented in Table 6. The agreement between simulated and observed O_3 is considered good, as indicated by lower values of RMSE (10.7–11 ppbv), MAB (6.5–7.1 ppbv), and NME (26.9%–27.8%). In contrast, the comparison for simulated NO_2 with observations shows higher NME (51.5%–52.7%). Figures S5(a–d) in supplementary material represent the absolute bias in the simulated annual mean of O_3 and NO_2 at the surface from experiment ~~wLNOx~~LNOx-CTH and LNOx-ICEFLUX, compared to the observations at ~~stations~~available stations over the NH. The simulated O_3 and NO_2 mixing ratio is close enough to the observations at most of the stations over Europe and China, and also over the USA for O_3 and Canada and south America for NO_2. Higher bias for O_3 is, nonetheless, observed at stations over Canada, South America and ~~northern and~~ few stations over eastern China. ~~The statistical analyses are done and presented in Table 6. The agreement between simulated and observed O_3 is considered good, as indicated by low values of RMSE (10.90 ppbv), MAB (5.63 ppbv), and NME (13.95%). In contrast, the comparison for NO_2 is moderately acceptable, with a slightly higher NME of 27.46%.~~ However, the inclusion of LNOx does not significantly impact the statistical scores~~when comparing surface mixing ratios with observations~~. A detailed analysis of the altitude-wise changes in the mixing ratio of O_3, due to the impact of LNOx, is therefore necessary and ~~is~~ has already been discussed in the ~~next section~~Sections 3.3.1 and 3.3.2.

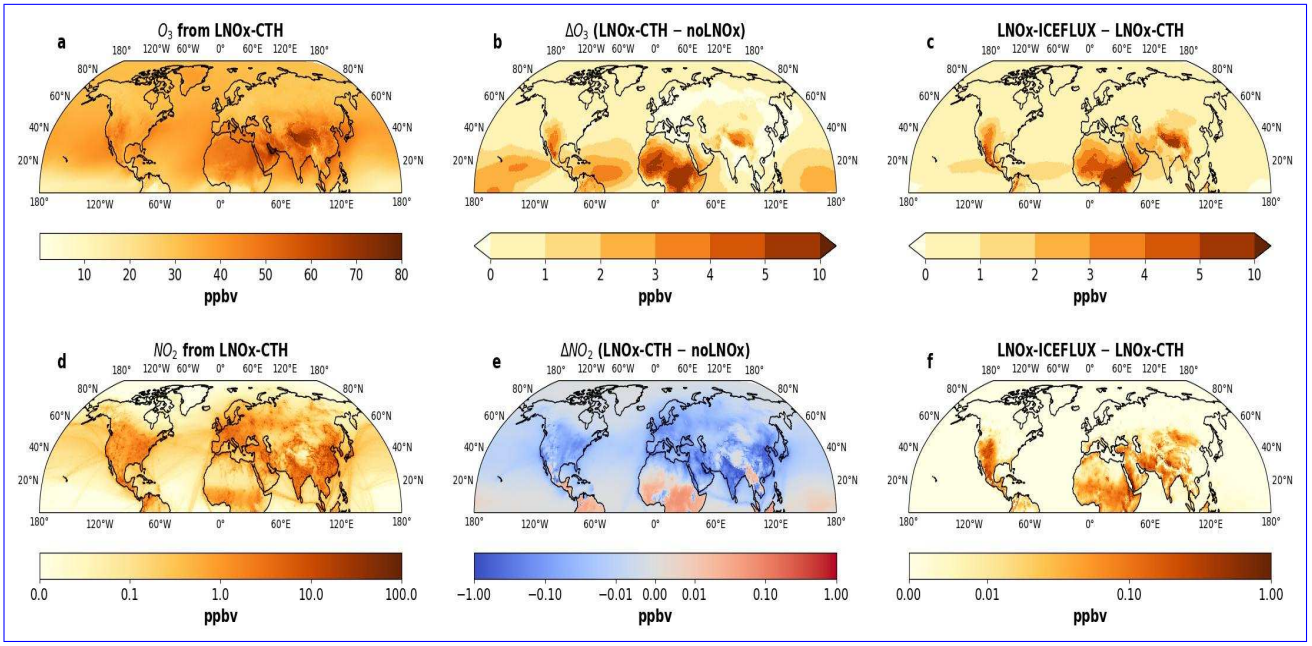

Figure 11. (a, d) Spatial distribution of annual mean mixing ratio in ppbv at the surface over NH from experiment LNOx-CTH for (a) O_3, (d) NO_2; (b, e) changes in mixing ratio at the surface due to inclusion of LNOx emissions for (b) O_3, (e) NO_2, positive and negative values show an increase and decrease, respectively; (c, f) differences in mixing ratio at the surface from experiment LNOx-ICEFLUX w. r. t. LNOx-CTH for (c) O_3, (f) NO_2.

Table 6. Statistical analysis comparing simulated mixing ratio at surface to the ground-based observations for O_3 and NO_2

	Mean observed surface conc. over NH (ppbv)	Total number of stations	noLNOx			LNOx-CTH			LNOx-ICEFLUX		
			RMSE (ppbv)	MAB** (ppbv)	NME (%)	RMSE (ppbv)	MAB** (ppbv)	NME (%)	RMSE (ppbv)	MAB** (ppbv)	NME (%)
O_3	32.48	5185	10.9	6.5	27.3	10.7	6.5	26.9	11.0	7.1	27.8
NO_2	14.3	3857	9.2	6.4	51.5	9.3	6.6	52.7	9.3	6.6	52.7

**The positive and negative values of MAB represent respectively, modelled fields are higher and lower than the measurements.

3.5 ~~Vertical distribution of O_3: effect of LNOx~~

~~The increase in the annual mean of O_3 mixing ratio, due to the inclusion of LNOx in simulation wLNOx, with respect to that from simulation noLNOx, averaged over four altitude bands (998–900, 900–750, 750–500 and 500–200 hPa) is presented in Figure 4. The highest increase in simulated O_3 is observed at the altitude band 750–500 hPa, specifically over the tropics, by 10–20 ppbv. 6–12 ppbv increase over the tropics is also observed at the altitude bands 750–500 hPa and 500–200 hPa (upper troposphere). The increase is maximum over the northern part of South America, central Africa, the eastern part of China and the Maritime Continent in south-east Asia (Indonesia, Philippines and Malaysia). The above-mentioned regions with large increases in O_3, identified for all the altitude bands, are observed as regions with the largest convection depth and LNOx emissions (Banerjee et al., 2014). The changes in O_3 mixing ratio are low to negligible over mid-latitudes (30° N–60° N) and polar region (60° N–90° N). The percentage increase in the annual mean of O_3 mixing ratio due to the inclusion of LNOx in~~

the model, at selected latitude and altitude bands, is also presented in Table **??**. Inclusion of LNOx in the model calculation, overall increases tropospheric O_3, while it is considerably high in the mid and upper troposphere (750–200 hPa), where O_3 is elevated by 20%–35%, especially over the tropics, as the maximum lightning discharge is found over the tropical mid to upper troposphere (Luhar et al., 2024). A moderate (6%–9%) to low (1%–2%) increase in mid and upper tropospheric O_3 is observed over mid-latitudes followed by the polar region. The tropospheric O_3 burden over NH is 133.63 Tg as estimated from the simulation wLNOx and is increased by 15% with respect to noLNOx simulation (Table 8). The estimated O_3 burden from our study is close enough but slightly underestimated in comparison to the global burden calculated in previous modeling studies (308–337 Tg; Young et al. (2013); Banerjee et al. (2014); Luhar et al. (2021)).

Changes in the annual mean of O_3 mixing ratio due to inclusion of LNOx emissions at the altitude bands of (a) 998–900 hPa, (b) 900–750 hPa, (c) 750–500 hPa and (d) 500–300 hPa; positive and negative values represent the increase and decrease in the O_3 mixing ratio, respectively.

Vertical profile of annual mean of O_3 mixing ratio from noLNOx (red solid line) and wLNOx (blue solid line) simulations and comparison with the ozone sonde measurements (black solid line), averaged for the stations over the latitude bands (a) 0°–30° N, (b) 30° N–60° N and (c) 60° N–90° N; the black dashed lines indicate the 10 and 90 percentiles of the ozone sonde data.

Figure 6 represents the vertical profile of the annual mean of O_3 mixing ratio from noLNOx and wLNOx simulations and their comparison with the ozone sonde measurements, averaged for the stations over the latitude bands 0°–30° N, 30° N–60° N and 60° N–90° N. The simulated O_3 mixing ratio does not vary significantly up to 500 hPa, as also presented in Table **??**, whereas an increase in O_3 mixing ratio from the ozone sonde is observed along with increasing altitude. The upper tropospheric O_3 mixing ratio is slightly higher (by 15%–20%) than that observed at surface over the tropics, while it is 2–4 times higher over the mid-latitudes and polar region (Table **??**). The upper tropospheric O_3 over the polar region is also almost twice that over the tropics (Table **??**). It is visible in Figure 6, that the simulated O_3 mixing ratio from the wLNOx experiment, represents the same from ozone sonde adequately well, in mid to upper troposphere over tropics and near-surface over mid-latitudes and polar region. The simulated O_3 over the tropics, mostly lies between the 10th and 90th percentiles of the ozone sonde data, showing that the model predictions are within a reasonable range of the observed variability. However, simulated O_3 highly deviates from the ozone sonde measurements above 900 hPa (around 1000 m) over mid-latitude and polar regions. The sharp increase in O_3 above 900 hPa, is not captured in the simulated O_3 profile, even after including LNOx in the model calculation, explaining the underestimation of tropospheric O_3 burden in NH as mentioned above. The O_3 in the model consistently falls below the 10th percentile of the ozone sonde data at the free troposphere over mid-latitudes and the polar region, suggesting a systematic underestimation in the simulated O_3, specifically in polar region. The absolute bias in simulated O_3 from simulations noLNOx and wLNOx, with respect to observed data from ozone sonde at selected latitude and altitude bands, is also presented in Table **??**. The absolute bias in simulated O_3 in the mid to upper troposphere over tropics and mid-latitudes is reduced due to inclusion of LNOx in the model, but still shows an underestimation. The bias reduction is significantly larger over the tropics in comparison to mid-latitudes. It is evident that, the O_3 production efficiency from LNOx is comparatively higher in the mid to upper troposphere due to lower temperature, which is favourable for the longer lifetime of NOx and O_3 (Finney et al., 2014).

~~The high underestimation in the simulated upper tropospheric O_3 mixing ratio, especially over mid-latitudes and polar regions, is possibly due to inadequate vertical mixing and representation of convection in the model and lack in stratosphere-troposphere exchange (Allen et al., 2010, 2012).~~

~~Details of annual mean O_3 from experiment 'wLNOx', its changes due to inclusion of LNOx and evaluation of simulated O_3 from experiments 'noLNOx' and 'wLNOx' w. r. t. observed data from ozone sonde at selected latitude and altitude bands* ΔO_3 represents changes in O_3 from experiment 'wLNOx' w. r. t. that from experiment 'noLNOx'; positive and negative values represent the increase and decrease in O_3 mixing ratio, respectively.** Reduction in absolute biases in the experiment 'wLNOx' w.r.t. 'noLNOx' (i) $\geq$3 ppbv and $\leq$6 ppbv: bold (for lower bias); (ii) $\geq$6 ppbv: bold, italics (for lower bias); positive and negative values of absolute bias show that the simulated O_3 is higher and lower than the measurements, respectively; correlation between the simulated and observed O_3 mixing ratio is estimated over space and time, aggregating stations in each latitude-altitude band and comparing values over time.~~

~~The correlation between simulated and ozone sonde-derived O_3 (represented in Table **??**) is strong only at lower altitudes over tropics and mid-latitudes and at upper troposphere over mid-latitudes and polar region and is not much affected due to the inclusion of LNOx. The correlation is weak in the mid to upper troposphere over the tropics despite of improvement in O_3 mixing ratio, suggesting that the model is not accurately capturing the observed variations and patterns in the O_3 data. This may indicate a limitation in the representation of the transport processes in model and a lack in emissions, especially during the biomass-burning seasons (von Kuhlmann et al., 2003).~~

3.5 Impacts on tropospheric OH burden and CH_4 lifetime

~~In the present study, we~~ We also have evaluated the effects of LNOx on tropospheric chemistry in terms of changes in the burden of a major oxidant (OH) and the lifetime of trace gas CH_4. Table 7 illustrates the concentration of OH from experiment ~~wLNOx and the increase~~ LNOx-CTH and the changes in concentration of OH ~~,~~ with respect to that from noLNOx averaged over selected latitude and altitude bands. The ~~highest OH concentration is observed at the tropical mid troposphere (21–27 $\times$ 10^5 molecules cm^{-3}).~~ OH concentration from the LNOx-ICEFLUX is also compared with that from LNOx-CTH in Table 7. The OH concentration in our study, over the tropics~~is almost 2–3 times and 8–10~~ , is almost twice and 6–7 times higher than that over mid-latitudes and polar regions, respectively~~. The OH concentration from our study is~~ , which is consistent with the study by Mao et al. (2021). Again these concentrations are close enough to those values obtained in a multi-model study by Naik et al. (2013), but shows a higher OH concentration at tropical mid-troposphere ~~than the surface~~(22–26 $\times$ 10^5 molecules cm^{-3}), unlike the ~~multi-model study. While the~~ studies by Naik et al. (2013); Luhar et al. (2021)~~, exhibit higher OH concentration at the surface than mid and upper troposphere , on the contrary higher concentration is observed in upper troposphere from the study by Banerjee et al. (2014).~~ Higher OH concentration in the upper troposphere is reported by Banerjee et al. (2014), due to transportation of water vapour through convection to the upper troposphere promoting the OH production due to reaction of exited state oxygen with water vapour. The annual mean OH concentration over NH, from our study~~is 14~~ , is 14.5 $\times$ 10^5 and 15.4 $\times$ 10^5 molecules cm^{-3} ~~, which is around 19~~from LNOx-CTH and LNOx-ICEFLUX, respectively, being 6.6% and 13.2% higher than that obtained from noLNOx simulation (Table 8). The annual ~~average~~ mean OH concentration is higher by

2630%–38% in comparison to the multi-model mean obtained from ACCMIP simulations ($11.1 \pm 1.8 \times 10^5$ molecules cm^{-3}; Naik et al., 2013; Voulgarakis et al., 2013). We find an increase in OH concentration due to LNOx, which is again the largest over mid and upper free troposphere at tropics (59%–6511%–28%), followed by mid-latitude and polar regions mid-latitudes (Table 7). A warmer atmosphere 5%–7% higher OH concentration is also observed from LNOx-ICEFLUX in comparison to that from LNOx-CTH at the free troposphere. A warmer atmosphere at tropics and high humidity influence an favour the increase in OH and a faster OH to CH_4 reaction, causing a shorter CH_4 lifetime at these regions (Voulgarakis et al., 2013). The geographical distribution of changes in OH due to lightning is usually effected by the lightning parameterization used (Gordillo-Vázquez et al., 2019). The spatial distribution of changes in simulated OH concentration from LNOx-CTH w. r. t. noLNOx and from LNOx-ICEFLUX w. r. t. LNOx-CTH, at selected altitude bands, are also presented, respectively in Figures S6 and S7 in the supplementary material. The OH burden over NH is increased to 0.091 Gg, from 0.065 Gg, due to the inclusion of LNOx by 14% and 24% in LNOx-CTH and LNOx-ICEFLUX, respectively, from 0.082 Gg, estimated in simulation noLNOx (Table 8). In our study, we have estimated CH_4 lifetime (τ_{CH_4}) due to chemical loss, mainly due to reaction with OHand the . The average lifetime over NH is 4.89 are 4.84 and 4.5 years, as obtained from experiment wLNOx. The lifetime of CH_4 is reduced by 24respectively from experiments LNOx-CTH and LNOx-ICEFLUX, which are reduced respectively by 11% and 17% compared to the estimate from the noLNOx simulation (Table 8), evidencing that the increase in OH burden due to LNOx decreases the CH_4 lifetime. The CH_4 lifetime as estimated from previous modeling modelling studies, is within a range of 7–14 years (Naik et al., 2013; Lelieveld et al., 2016) and is visibly underestimated in our study. It is to be noted in this regard that, the The underestimation in CH_4 anthropogenic emissions are not taken into account in the model and CH_4 concentration comes from chemical boundary conditions. Hence, it is necessary to evaluate the sensitivity lifetime in our study is due to the overestimation of OH concentrations, which promote the oxidation of CH_4lifetime estimates toward the initial chemical boundary conditions. Additionally, there is a need for further investigation into the source and sink pathways of OH in the CHIMERE model to improve the estimation of the OH burden and , reducing the burden and increasing the chemical loss of CH_4, even in the absence of LNOx. Therefore, the underestimated CH_4 lifetime . in the present study is not attributed to LNOx but likely stems from other factors including issues related to deficiencies in the chemistry or photolysis schemes. Addressing and resolving this issue will require further investigation in future studies. The CH_4 lifetime is underestimated especially over tropics showing values of 2–4 years (Figure S8 in supplementary material). The lifetime increases with higher latitudes and is maximum at polar region (40–60 years), which matches well with the estimated values from the study by Lelieveld et al. (2016) , over higher latitudes (45°–90°N).

Conclusion

In the present study , NOx from lightning This study evaluates the incorporation of lightning-produced NOx (LNOx) has been incorporated in the into the CHIMERE chemistry-transport model CHIMERE and its effect to assess its impact on tropospheric ozone (O_3) is studied. The LNOx is estimated with a classical over the Northern Hemisphere (NH). A classical lightning parameterization based on cloud top height (CTH), developed by Price and Rind (1992). A correction factor of 1/5 is

~~OH concentration averaged over selected latitude and altitude bands for simulations wLNOx and percentage increase in OH concentration w. r. t. noLNOx~~

Table 7. Analysis of simulated OH concentration averaged over selected latitude and altitude bands. ΔOH represents changes in OH from experiment 'LNOx-CTH' w. r. t. that from experiment 'noLNOx'; positive and negative values represent the increase and decrease in OH concentration, respectively.

~~† ΔOH represents changes in OH from experiment 'wLNOx' w. r. t. that from experiment 'noLNOx'; positive and negative values represent the increase and decrease in OH concentration, respectively.~~

Latitude band	0°–30° N	30° N–60° N	60° N–90° N	0°–30° N	30° N–60° N	60° N–90° N	0°–30° N	30° N–60° N	60° N–90° N
Altitude band (hPa)	OH concentration (10^5 molecules cm^{-3}) from LNOx-CTH			ΔOH (%)			LNOx-ICEFLUX − LNOx-CTH (%)		
500–200	15.1	7.3	2.6	20.8	7.3	−3.7	5.2	2.6	1.5
750–500	26.0	11.3	3.1	28.7	8.6	−6.1	7.6	3.5	1.7
900–750	22.4	11.9	3.2	11.4	0	−3.0	5.8	2.6	1.1
998–900	19.5	13.4	2.8	2.1	−2.9	−3.7	4.2	1.9	0.8

Table 8. Tropospheric O_3, NO_2, OH burden and CH_4 lifetime from simulation experiments. The numbers within parenthesis represent the tropospheric O_3 burden over the domain from 0°–60°N.

~~noLNOx wLNOx~~

	noLNOx	LNOx-CTH	LNOx-ICEFLUX
O_3 burden (Tg)†	164 (138)	176 (150)	182 (155)
NO_2 burden (Gg)††	146	146	172
OH concentration (molecules cm^{-3})	13.6×10^5	14.5×10^5	15.4×10^5
OH burden (Gg)	0.082	0.094	0.102
CH_4 lifetime due to chemical loss (yr)	5.45	4.84	4.5

†Tropospheric O_3 burden ~~(Tg) 116.53 133.63 OH concentration (molecules cm^{-3}) 11.72×10^5 14.01×10^5 OH burden (Gg) 0.065 0.091 CH_4 lifetime due to chemical loss (yr) 6.45 4.89~~ from OMI/MLS, estimated over the domain 0°–60°N, is 159 Tg.

††Tropospheric NO_2 burden over NH from OMI is 164 Gg.

~~applied over the land grids to exhibit the modelled flash rate close to the satellite-based measurements (experiment: wLNOx). The estimated annual mean of flash rate from our study is highest over tropical lands (0.8–1.5 flashes km^{-2} day~~, is applied (experiment: LNOx-CTH) with modifications to better align modelled flash rates over lands and oceans to satellite observations. Additionally, flash rates are computed using an updated ice flux based lightning scheme (experiment: LNOx-ICEFLUX; Finney et al., 2014). We perform a detailed evaluation of model simulations, integrating in situ measurements and satellite observations to critically assess the reliability and applicability of these parameterizations. The annual flash frequencies over the NH are 20.7 and 21.6 flashes s^{-1} ~~) and provides 5–6 times higher values over the tropics, in comparison to observations. The total NO emissions from lightning (LNO) is estimated as 8.82~~ as estimated from the LNOx-CTH and LNOx-ICEFLUX experiments, respectively. For LNOx-ICEFLUX, a correction factor of 5 is applied to the simulated annual flash frequencies. The estimated LNOx emissions are 2.8 and 3.1 Tg N yr^{-1} ~~over the northern hemisphere (NH) and lies within the wide range of model-estimated LNO emissions from previous studies. The high uncertainty in modelled flash rates~~from LNOx-CTH and LNOx-ICEFLUX experiments, respectively. Our study provides a comparative assessment of these two lightning parameterizations, evaluating their influence on modelled lightning flashes, LNOx emissions and ~~insufficiently simulated seasonality in flash rate, estimated~~

using the over-simplified CTH parameterization scheme, drive us to investigate more recent parameterization methods for lightning.

To examine the effects of LNOx on tropospheric tropospheric distribution of O_3 mixing ratio, we have conducted simulations without (experiment: noLNOx) and with (experiment: wLNOx) LNOx emissions. After comparing the results from these experiments, an increase of 2–5 ppbv in and trace gases, with implications for improving both the parameterizations and the overall model.

The major outcomes from our study are delineated here. Annual flash rates in tropical land and NH regions from both experiments, as well as in mid-latitudes from LNOx-ICEFLUX, show good agreement with satellite observations. Both the ICEFLUX and CTH schemes as implemented in CHIMERE, reproduce the seasonal cycle of lightning flash rates correctly over the annual mean of O_3 mixing ratio at the surface, is observed due to the inclusion of LNOx, over most of the NH region. The increase is 2–3 times larger over the tropical lands, where a high lightning flash rate is found. The change in simulated NO_2 at the surface is negligible in comparison and exhibits a moderately acceptable agreement with the ground-based observations at available stations. The simulated lands. LNOx emission peak during May–August, contributing 60%–70% of the total annual emissions, with most emissions concentrated in the tropics and mid-latitudes, and 60%–65% occurring in the mid-tropospheric region. The inclusion of LNOx emissions in CHIMERE significantly improves the simulated tropospheric O_3 at surface is however in good agreement with observations, showing comparatively lower absolute mean bias and errors. There is an overall increase in O_3 observed in the distribution, particularly in the free troposphere over the tropics. A significant bias at the upper troposphere due to the inclusion of LNOx and shows a maximum increase in the mid to upper troposphere , specifically over the tropics, where extreme lightning discharge occurs. We successfully simulate the mid to upper tropospheric and lower stratosphere at higher latitudes, however highlights the necessity of improving the representation of stratosphere-troposphere exchange processes in the model. The model adequately simulates the O_3 over the tropical region in experiment wLNOx, reducing the absolute bias in simulated O_3 in comparison to ozone sonde measurements. The tropospheric and NO_2 burden over the NH compared to satellite observations, showing a 7%–11% increase in O_3 burden over NH is increased from 116.53 Tg to 133.63 Tgfrom 164 Tg, due to the inclusion of LNOx. The high underestimation in simulated O_3, at free troposphere over mid-latitudes and polar regions, indicates inadequate vertical mixing and representation of convection and stratosphere-troposphere exchangeLNOx.

In our study , we also have shown the impact of LNOx on hydroxyl radical (OH) burden and lifetime of trace gas methane (CH_4). The average tropospheric OH concentration is estimated as Additionally, it leads to a 14×10^5 molecules cm^{-3} over NH, which is highest over the tropics, especially in the mid-troposphere. The tropospheric OH concentration is slightly higher than that estimated from previous model-based studies and the CH_4 lifetime is reduced to a comparatively lower value of 4.89 years. Here, we estimate the CH_4 lifetime due to chemical loss through the reaction with OH radical. Hence, in the presence of LNOx, the OH burden increases by 40% and the average lifetime of CH%–24% increase in OH burden from 0.082 Gg and a 11%–17% reduction in CH_4 reduces by 24% over the NH. Our studyfurther suggests investigating the effects of initial chemical boundary conditions and lifetime compared to the without LNOx scenario, though there remains scope for refining OH-related chemistry.

Our study underscores that, despite its simple representation, the ~~source–sink pathways of OH in the CHIMERE model for further improvement in OH burden and CH_4 lifetime estimation~~CTH scheme better captures the spatial variability of flashes compared to satellite observations, outperforming the ICEFLUX scheme. However, the limitations of the CTH scheme in capturing mid-latitude flashes underscore the efficacy of the ICEFLUX scheme in these areas. Additionally, improving convective parameterization is crucial for better representation of oceanic flash rates. The ICEFLUX scheme also faces challenges in accurately simulating high-energy, less frequent flashes over oceans, emphasizing the need to incorporate additional factors alongside ice flux. The challenges to constrain parameters, such as cloud ice content and updraft mass flux, which are utilized in flux-based lightning schemes, continue due to limited available observations. A recent study by Cummings et al. (2024) , which have evaluated eighteen lightning parameterization schemes, demonstrates that those based on storm kinematics and structure performed better than the microphysical schemes, in their study. Developing integrated parameterizations that incorporate both storm kinematics and microphysical processes, along with improved observational constraints, may provide a more robust and accurate representation of lightning flash rates, particularly in complex storm environments.

Code and data availability. The CHIMERE model (v2023r2) is available on the website at https://www.lmd.polytechnique.fr/chimere/. The in situ measurements and satellite data used in the study are all freely downloadable from cited URLs.

Author contributions. SG analysed the model output and data, downloaded satellite data, made plots, conceptualised and prepared a original version of the manuscript. AC performed the simulations and contributed to the measurement data collection. All co-authors have participated in conceptualisation of the study, the interpretation and discussion of the results, and the drafting of the final manuscript.

Competing interests. The authors declare that they have no conflict of interest.

Acknowledgements. This study was supported by the Agence de l'Environnement et de la Maîtrise de l'Energie (ADEME) within the framework of the ESCALAIR project (grant: 2162D0017). We also acknowledge the use of computational resources provided by the GENCI GEN10274 project.

References

Akimoto, H. and Tanimoto, H.: Rethinking of the adverse effects of NOx-control on the reduction of methane and tropospheric ozone–challenges toward a denitrified society, Atmospheric Environment, 277, 119 033, https://doi.org/10.1016/j.atmosenv.2022.119033, 2022.

Albrecht, R. I., Goodman, S. J., Buechler, D. E., Blakeslee, R. J., and Christian, H. J.: Where Are the Lightning Hotspots on Earth?, Bulletin of the American Meteorological Society, 97, 2051–2068, https://doi.org/10.1175/BAMS-D-14-00193.1, 2016.

Alfaro, S. C. and Gomes, L.: Modeling mineral aerosol production by wind erosion: Emission intensities and aerosol size distributions in source areas, Journal of Geophysical Research: Atmospheres, 106, 18 075–1808, https://doi.org/10.1029/2000JD900339, 2001.

Allen, D., Pickering, K., Stenchikov, G., Thompson, A., and Kondo, Y.: A three-dimensional total odd nitrogen (NOy) simulation during SONEX using a stretched-grid chemical transport model, Journal of Geophysical Research: Atmospheres, 105, 3851–3876, https://doi.org/10.1029/1999JD901029, 2000.

Allen, D., Pickering, K., Duncan, B., and Damon, M.: Impact of lightning NO emissions on North American photochemistry as determined using the Global Modeling Initiative (GMI) model, Journal of Geophysical Research: Atmospheres, 115, 2010.

Allen, D. J. and Pickering, K. E.: Evaluation of lightning flash rate parameterizations for use in a global chemical transport model, Journal of Geophysical Research: Atmospheres, 107, ACH–15, https://doi.org/10.1029/2002JD002066, 2002.

Allen, D. J., Pickering, K. E., Pinder, R. W., Henderson, B. H., Appel, K. W., and Prados, A.: Impact of lightning-NO on eastern United States photochemistry during the summer of 2006 as determined using the CMAQ model, Atmospheric Chemistry and Physics, 12, 1737–1758, https://doi.org/10.5194/acp-12-1737-2012, 2012.

Arndt, J. A., Aulinger, A., and Matthias, V.: Quantification of lightning-induced nitrogen oxide emissions over Europe, Atmospheric Environment, 202, 128–141, 2019.

Banerjee, A., Archibald, A. T., Maycock, A. C., Telford, P., Abraham, N. L., Yang, X., Braesicke, P., and Pyle, J. A.: Lightning NOx, a key chemistry–climate interaction: impacts of future climate change and consequences for tropospheric oxidising capacity, Atmospheric Chemistry and Physics, 14, 9871–9881, 2014.

Bessagnet, B., Menut, L., Curci, G., Hodzic, A., Guillaume, B., Liousse, C., Moukhtar, S., Pun, B., Seigneur, C., and Schulz, M.: Regional modeling of carbonaceous aerosols over Europe–focus on secondary organic aerosols, Journal of Atmospheric Chemistry, 61, 175–202, https://doi.org/10.1007/s10874-009-9129-2, 2008.

Blakeslee, R. J., Lang, T. J., Koshak, W. J., Buechler, D., Gatlin, P., Mach, D. M., Stano, G. T., Virts, K. S., Walker, T. D., Cecil, D. J., Ellett, W., Goodman, S. J., Harrison, S., Hawkins, D. L., Heumesser, M., Lin, H., Maskey, M., Schultz, C. J., Stewart, M., Bateman, M., Chanrion, O., and Christian, H.: Three Years of the Lightning Imaging Sensor Onboard the International Space Station: Expanded Global Coverage and Enhanced Applications, Journal of Geophysical Research: Atmospheres, 125, e2020JD032 918, https://doi.org/10.1029/2020JD032918, 2020.

Boccippio, D. J.: Lightning Scaling Relations Revisited, Journal of the Atmospheric Sciences, 59, 1086–1104, https://doi.org/10.1175/1520-0469(2002)059<1086:LSRR>2.0.CO;2, 2002.

Boccippio, D. J., Cummins, K. L., Christian, H. J., and Goodman, S. J.: Combined satellite-and surface-based estimation of the intracloud–cloud-to-ground lightning ratio over the continental United States, Monthly Weather Review, 129, 108–122, https://doi.org/10.1175/1520-0493(2001)129<0108:CSASBE>2.0.CO;2, 2001.

Bucsela, E., Krotkov, N., Celarier, E., Lamsal, L., Swartz, W., Bhartia, P., Boersma, K., Veefkind, J., Gleason, J., and Pickering, K.: A new stratospheric and tropospheric NO 2 retrieval algorithm for nadir-viewing satellite instruments: applications to OMI, Atmospheric Measurement Techniques, 6, 2607–2626, https://doi.org/10.5194/amt-6-2607-2013, 2013.

Bucsela, E. J., Pickering, K. E., Allen, D. J., Holzworth, R. H., and Krotkov, N. A.: Midlatitude Lightning NOx Production Efficiency Inferred From OMI and WWLLN Data, Journal of Geophysical Research: Atmospheres, 124, 13 475–13 497, https://doi.org/10.1029/2019JD030561, 2019.

Burkholder, J. B., Sander, S. P., Abbatt, J., Barker, J. R., Cappa, C., Crounse, J. D., Dibble, T. S., Huie, R. E., Kolb, C. E., Kurylo, M. J., Orkin, V. L., Percival, C. J., Wilmouth, D. M., and Wine, P. H.: Chemical Kinetics and Photochemical Data for Use in Atmospheric Studies, Evaluation No. 19, Jet Propulsion Laboratory, Pasadena, http://jpldataeval.jpl.nasa.gov, 2019.

Butler, T., Lupascu, A., and Nalam, A.: Attribution of ground-level ozone to anthropogenic and natural sources of nitrogen oxides and reactive carbon in a global chemical transport model, Atmospheric Chemistry and Physics, 20, 10 707–10 731, https://doi.org/10.5194/acp-20-10707-2020, 2020.

Carey, L. D., Koshak, W., Peterson, H., and Mecikalski, R. M.: The kinematic and microphysical control of lightning rate, extent, and NO production, Journal of Geophysical Research: Atmospheres, 121, 7975–7989, https://doi.org/10.1002/2015JD024703, 2016.

Cecil, D. J., Buechler, D. E., and Blakeslee, R. J.: Gridded lightning climatology from TRMM-LIS and OTD: Dataset description, Atmospheric Research, 135, 404–414, https://doi.org/10.1016/j.atmosres.2012.06.028, 2014.

Cheng, P., Pour-Biazar, A., Wu, Y., Kuang, S., McNider, R. T., and Koshak, W. J.: Utility of Geostationary Lightning Mapper-derived lightning NO emission estimates in air quality modeling studies, Atmospheric Chemistry and Physics, 24, 41–63, https://doi.org/10.5194/acp-24-41-2024, 2024.

Chin, M., Ginoux, P., Kinne, S., Torres, O., Holben, B. N., Duncan, B. N., Martin, R. V., Logan, J. A., Higurashi, A., and Nakajima, T.: Tropospheric Aerosol Optical Thickness from the GOCART Model and Comparisons with Satellite and Sun Photometer Measurements, Journal of the Atmospheric Sciences, 59, 461–483, https://doi.org/10.1175/1520-0469(2002)059<0461:TAOTFT>2.0.CO;2, 2002.

Choi, Y., Wang, Y., Zeng, T., Martin, R. V., Kurosu, T. P., and Chance, K.: Evidence of lightning NOx and convective transport of pollutants in satellite observations over North America, Geophysical Research Letters, 32, https://doi.org/10.1029/2004GL021436, 2005.

Christian, H. J. and Petersen, W.: Global lightning activity, in: Conference on Meteorological Applications of Lightning Data, 85th AMS Annual Meeting, San Diego, CA, pp. 10–12, 2005.

Clark, S. K., Ward, D. S., and Mahowald, N. M.: Parameterization-based uncertainty in future lightning flash density, Geophysical Research Letters, 44, 2893–2901, https://doi.org/10.1002/2017GL073017, 2017.

Cooper, M. J., Martin, R. V., Hammer, M. S., Levelt, P. F., Veefkind, P., Lamsal, L. N., Krotkov, N. A., Brook, J. R., and McLinden, C. A.: Global fine-scale changes in ambient NO2 during COVID-19 lockdowns, Nature, 601, 380–387, https://doi.org/10.1038/s41586-021-04229-0, 2022.

Cummings, K., Pickering, K., Barth, M., Bela, M., Li, Y., Allen, D., Bruning, E., MacGorman, D., Ziegler, C., Biggerstaff, M., et al.: Evaluation of lightning flash rate parameterizations in a cloud-resolved WRF-Chem simulation of the 29–30 May 2012 Oklahoma severe supercell system observed during DC3, Journal of Geophysical Research: Atmospheres, 129, e2023JD039 492, https://doi.org/10.1029/2023JD039492, 2024.

Dahlmann, K., Grewe, V., Ponater, M., and Matthes, S.: Quantifying the contributions of individual NOx sources to the trend in ozone radiative forcing, Atmospheric Environment, 45, 2860–2868, https://doi.org/10.1016/j.atmosenv.2011.02.071, 2011.

Després, B. and Lagoutière, F.: A non-linear anti-diffusive scheme for the linear advection equation, Comptes Rendus de l'Académie des Sciences-Series I-Mathematics, 328, 939–943, https://doi.org/10.1016/S0764-4442(99)80301-2, 1999.

Dufour, G., Hauglustaine, D., Zhang, Y., Eremenko, M., Cohen, Y., Gaudel, A., Siour, G., Lachatre, M., Bense, A., Bessagnet, B., et al.: Recent ozone trends in the Chinese free troposphere: role of the local emission reductions and meteorology, Atmospheric Chemistry and Physics, 21, 16 001–16 025, https://doi.org/10.5194/acp-21-16001-2021, 2021.

Erdmann, F., Defer, E., Caumont, O., Blakeslee, R. J., Pédeboy, S., and Coquillat, S.: Concurrent satellite and ground-based lightning observations from the Optical Lightning Imaging Sensor (ISS-LIS), the low-frequency network Meteorage and the SAETTA Lightning Mapping Array (LMA) in the northwestern Mediterranean region, Atmospheric Measurement Techniques, 13, 853–875, https://doi.org/10.5194/amt-13-853-2020, 2020.

Fehr, T., Höller, H., and Huntrieser, H.: Model study on production and transport of lightning-produced NOx in a EULINOX supercell storm, Journal of Geophysical Research: Atmospheres, 109, D09 102, https://doi.org/10.1029/2003JD003935, 2004.

Finney, D., Doherty, R., Wild, O., and Abraham, N. L.: The impact of lightning on tropospheric ozone chemistry using a new global lightning parametrisation, Atmospheric Chemistry and Physics, 16, 7507–7522, https://doi.org/10.5194/acp-16-7507-2016, 2016a.

Finney, D. L., Doherty, R. M., Wild, O., Huntrieser, H., Pumphrey, H. C., and Blyth, A. M.: Using cloud ice flux to parametrise large-scale lightning, Atmospheric Chemistry and Physics, 14, 12 665–12 682, https://doi.org/10.5194/acp-14-12665-2014, 2014.

Finney, D. L., Doherty, R. M., Wild, O., Young, P. J., and Butler, A.: Response of lightning NOx emissions and ozone production to climate change: Insights from the Atmospheric Chemistry and Climate Model Intercomparison Project, Geophysical Research Letters, 43, 5492–5500, https://doi.org/10.1002/2016GL068825, 2016b.

Ghosh, A., Patra, P. K., Ishijima, K., Umezawa, T., Ito, A., Etheridge, D. M., Sugawara, S., Kawamura, K., Miller, J. B., Dlugokencky, E. J., Krummel, P. B., Fraser, P. J., Steele, L. P., Langenfelds, R. L., Trudinger, C. M., White, J. W. C., Vaughn, B., Saeki, T., Aoki, S., and Nakazawa, T.: Variations in global methane sources and sinks during 1910–2010, Atmospheric Chemistry and Physics, 15, 2595–2612, https://doi.org/10.5194/acp-15-2595-2015, 2015.

Ghosh, R., Pawar, S. D., Hazra, A., Wilkinson, J., Mudiar, D., Domkawale, M. A., Vani, K. G., and Gopalakrishnan, V.: Seasonal and Regional Distribution of Lightning Fraction Over Indian Subcontinent, Earth and Space Science, 10, e2022EA002 728, https://doi.org/10.1029/2022EA002728, 2023.

Goldenbaum, G. and Dickerson, R.: Nitric oxide production by lightning discharges, Journal of Geophysical Research: Atmospheres, 98, 18 333–18 338, https://doi.org/10.1029/93JD01018, 1993.

Gordillo-Vázquez, F. J., Pérez-Invernón, F. J., Huntrieser, H., and Smith, A. K.: Comparison of Six Lightning Parameterizations in CAM5 and the Impact on Global Atmospheric Chemistry, Earth and Space Science, 6, 2317–2346, https://doi.org/10.1029/2019EA000873, 2019.

Guenther, A. B., Jiang, X., Heald, C. L., Sakulyanontvittaya, T., Duhl, T., Emmons, L. K., and Wang, X.: The Model of Emissions of Gases and Aerosols from Nature version 2.1 (MEGAN2.1): an extended and updated framework for modeling biogenic emissions, Geoscientific Model Development, 5, 1471–1492, https://doi.org/10.5194/gmd-5-1471-2012, 2012.

Hasenkopf, C. A., Flasher, J. C., Veerman, O., and DeWitt, H. L.: OpenAQ: a platform to aggregate and freely share global air quality data, in: AGU Fall Meeting Abstracts, vol. 2015, pp. A31D–0097, 2015.

Hauglustaine, D. A., Balkanski, Y., and Schulz, M.: A global model simulation of present and future nitrate aerosols and their direct radiative forcing of climate, Atmospheric Chemistry and Physics, 14, 11 031–11 063, https://doi.org/10.5194/acp-14-11031-2014, 2014.

Holle, R. L., Cummins, K. L., and Brooks, W. A.: Seasonal, Monthly, and Weekly Distributions of NLDN and GLD360 Cloud-to-Ground Lightning, Monthly Weather Review, 144, 2855–2870, https://doi.org/10.1175/MWR-D-16-0051.1, 2016.

Inness, A., Ades, M., Agustí-Panareda, A., Barré, J., Benedictow, A., Blechschmidt, A.-M., Dominguez, J. J., Engelen, R., Eskes, H., Flemming, J., Huijnen, V., Jones, L., Kipling, Z., Massart, S., Parrington, M., Peuch, V.-H., Razinger, M., Remy, S., Schulz, M., and Suttie, M.: The CAMS reanalysis of atmospheric composition, Atmospheric Chemistry and Physics, 19, 3515–3556, https://doi.org/10.5194/acp-19-3515-2019, 2019.

Jourdain, L., Kulawik, S., Worden, H., Pickering, K., Worden, J., and Thompson, A.: Lightning NO x emissions over the USA constrained by TES ozone observations and the GEOS-Chem model, Atmospheric Chemistry and Physics, 10, 107–119, https://doi.org/10.5194/acp-10-107-2010, 2010.

Kang, D., Foley, K. M., Mathur, R., Roselle, S. J., Pickering, K. E., and Allen, D. J.: Simulating lightning NO production in CMAQv5. 2: performance evaluations, Geoscientific model development, 12, 4409–4424, https://doi.org/10.5194/gmd-12-4409-2019, 2019.

Kang, D., Mathur, R., Pouliot, G. A., Gilliam, R. C., and Wong, D. C.: Significant ground-level ozone attributed to lightning-induced nitrogen oxides during summertime over the Mountain West States, NPJ climate and atmospheric science, 3, 6, https://doi.org/10.1038/s41612-020-0108-2, 2020.

Koshak, W., Peterson, H., Biazar, A., Khan, M., and Wang, L.: The NASA Lightning Nitrogen Oxides Model (LNOM): Application to air quality modeling, Atmospheric Research, 135-136, 363–369, https://doi.org/10.1016/j.atmosres.2012.12.015, 2014.

Krider, E., Dawson, G., and Uman, M.: Peak power and energy dissipation in a single-stroke lightning flash, Journal of Geophysical Research, 73, 3335–3339, https://doi.org/10.1029/JB073i010p03335, 1968.

Labrador, L. J., von Kuhlmann, R., and Lawrence, M. G.: The effects of lightning-produced NOx and its vertical distribution on atmospheric chemistry: sensitivity simulations with MATCH-MPIC, Atmospheric Chemistry and Physics, 5, 1815–1834, https://doi.org/10.5194/acp-5-1815-2005, 2005.

Lachatre, M., Mailler, S., Menut, L., Turquety, S., Sellitto, P., Guermazi, H., Salerno, G., Caltabiano, T., and Carboni, E.: New strategies for vertical transport in chemistry transport models: application to the case of the Mount Etna eruption on 18 March 2012 with CHIMERE v2017r4, Geoscientific Model Development, 13, 5707–5723, https://doi.org/10.5194/gmd-13-5707-2020, 2020.

Lamsal, L. N., Krotkov, N. A., Vasilkov, A., Marchenko, S., Qin, W., Yang, E.-S., Fasnacht, Z., Joiner, J., Choi, S., Haffner, D., et al.: Ozone Monitoring Instrument (OMI) Aura nitrogen dioxide standard product version 4.0 with improved surface and cloud treatments, Atmospheric Measurement Techniques, 14, 455–479, https://doi.org/10.5194/amt-14-455-2021, 2021.

Lelieveld, J. and Dentener, F. J.: What controls tropospheric ozone?, Journal of Geophysical Research: Atmospheres, 105, 3531–3551, https://doi.org/10.1029/1999JD901011, 2000.

Lelieveld, J., Gromov, S., Pozzer, A., and Taraborrelli, D.: Global tropospheric hydroxyl distribution, budget and reactivity, Atmospheric Chemistry and Physics, 16, 12 477–12 493, https://doi.org/10.5194/acp-16-12477-2016, 2016.

Levelt, P. F., Joiner, J., Tamminen, J., Veefkind, J. P., Bhartia, P. K., Stein Zweers, D. C., Duncan, B. N., Streets, D. G., Eskes, H., van der A, R., et al.: The Ozone Monitoring Instrument: overview of 14 years in space, Atmospheric Chemistry and Physics, 18, 5699–5745, https://doi.org/10.5194/acp-18-5699-2018, 2018.

Li, M., Mao, J., Chen, S., Bian, J., Bai, Z., Wang, X., Chen, W., and Yu, P.: Significant contribution of lightning NOx to summertime surface O3 on the Tibetan Plateau, Science of The Total Environment, 829, 154 639, https://doi.org/10.1016/j.scitotenv.2022.154639, 2022.

Liaskos, C. E., Allen, D. J., and Pickering, K. E.: Sensitivity of tropical tropospheric composition to lightning NOx production as determined by replay simulations with GEOS-5, Journal of Geophysical Research: Atmospheres, 120, 8512–8534, https://doi.org/10.1002/2014JD022987, 2015.

Luhar, A. K., Galbally, I. E., Woodhouse, M. T., and Abraham, N. L.: Assessing and improving cloud-height-based parameterisations of global lightning flash rate, and their impact on lightning-produced NO x and tropospheric composition in a chemistry–climate model, Atmospheric Chemistry and Physics, 21, 7053–7082, https://doi.org/10.5194/acp-21-7053-2021, 2021.

Luhar, A. K., Jones, A. C., and Wilkinson, J. M.: Quantifying the impact of global nitrate aerosol on tropospheric composition fields and its production from lightning NOx, Atmospheric Chemistry and Physics, 24, 14 005–14 028, https://doi.org/10.5194/acp-24-14005-2024, 2024.

Luo, C., Wang, Y., and Koshak, W. J.: Development of a self-consistent lightning NOx simulation in large-scale 3-D models, Journal of Geophysical Research: Atmospheres, 122, 3141–3154, https://doi.org/10.1002/2016JD026225, 2017.

Mailler, S., Menut, L., di Sarra, A. G., Becagli, S., Di Iorio, T., Bessagnet, B., Briant, R., Formenti, P., Doussin, J.-F., Gómez-Amo, J. L., Mallet, M., Rea, G., Siour, G., Sferlazzo, D. M., Traversi, R., Udisti, R., and Turquety, S.: On the radiative impact of aerosols on photolysis rates: comparison of simulations and observations in the Lampedusa island during the ChArMEx/ADRIMED campaign, Atmospheric Chemistry and Physics, 16, 1219–1244, https://doi.org/10.5194/acp-16-1219-2016, 2016.

Mao, J., Zhao, T., Keller, C. A., Wang, X., McFarland, P. J., Jenkins, J. M., and Brune, W. H.: Global Impact of Lightning-Produced Oxidants, Geophysical Research Letters, 48, e2021GL095 740, https://doi.org/10.1029/2021GL095740, 2021.

Maseko, B., Feig, G., and Burger, R.: Estimating lightning NOx production over South Africa, South African Journal of Science, 117, 1–11, https://doi.org/10.17159/sajs.2021/8035, 2021.

Menut, L., Bessagnet, B., Khvorostyanov, D., Beekmann, M., Blond, N., Colette, A., Coll, I., Curci, G., Foret, G., Hodzic, A., Mailler, S., Meleux, F., Monge, J. L., Pison, I., Siour, G., Turquety, S., Valari, M., Vautard, R., and Vivanco, M. G.: CHIMERE 2013: a model for regional atmospheric composition modelling, Geoscientific Model Development, 6, 981–1028, https://doi.org/10.5194/gmd-6-981-2013, 2013.

Menut, L., Bessagnet, B., Mailler, S., Pennel, R., and Siour, G.: Impact of lightning NOx emissions on atmospheric composition and meteorology in Africa and Europe, Atmosphere, 11, 1128, https://doi.org/10.3390/atmos11101128, 2020a.

Menut, L., Bessagnet, B., Siour, G., Mailler, S., Pennel, R., and Cholakian, A.: Impact of lockdown measures to combat Covid-19 on air quality over western Europe, Science of The Total Environment, 741, 140 426, https://doi.org/10.1016/j.scitotenv.2020.140426, 2020b.

Menut, L., Bessagnet, B., Briant, R., Cholakian, A., Couvidat, F., Mailler, S., Pennel, R., Siour, G., Tuccella, P., Turquety, S., and Valari, M.: The CHIMERE v2020r1 online chemistry-transport model, Geoscientific Model Development, 14, 6781–6811, https://doi.org/10.5194/gmd-14-6781-2021, 2021.

Menut, L., Cholakian, A., Pennel, R., Siour, G., Mailler, S., Valari, M., Lugon, L., and Meurdesoif, Y.: The CHIMERE chemistry-transport model v2023r1, Geoscientific Model Development Discussions, 2024, 1–44, https://doi.org/10.5194/gmd-17-5431-2024, 2024.

Michalon, N., Nassif, A., Saouri, T., Royer, J. F., and Pontikis, C. A.: Contribution to the climatological study of lightning, Geophysical Research Letters, 26, 3097–3100, https://doi.org/10.1029/1999GL010837, 1999.

Miyazaki, K., Eskes, H. J., Sudo, K., and Zhang, C.: Global lightning NOx production estimated by an assimilation of multiple satellite data sets, Atmospheric Chemistry and Physics, 14, 3277–3305, https://doi.org/10.5194/acp-14-3277-2014, 2014.

Monahan, E. C.: The Ocean as a Source for Atmospheric Particles, pp. 129–163, Springer Netherlands, https://doi.org/10.1007/978-94-009-4738-2_6, 1986.

Murray, L. T.: Lightning NOx and impacts on air quality, Current Pollution Reports, 2, 115–133, 2016.

Murray, L. T., Jacob, D. J., Logan, J. A., Hudman, R. C., and Koshak, W. J.: Optimized regional and interannual variability of lightning in a global chemical transport model constrained by LIS/OTD satellite data, Journal of Geophysical Research: Atmospheres, 117, 2012.

Murray, L. T., Logan, J. A., and Jacob, D. J.: Interannual variability in tropical tropospheric ozone and OH: The role of lightning, Journal of Geophysical Research: Atmospheres, 118, 11–468, 2013.

Murray, L. T., Fiore, A. M., Shindell, D. T., Naik, V., and Horowitz, L. W.: Large uncertainties in global hydroxyl projections tied to fate of reactive nitrogen and carbon, Proceedings of the National Academy of Sciences, 118, e2115204 118, https://doi.org/10.1073/pnas.2115204118, 2021.

Naik, V., Voulgarakis, A., Fiore, A. M., Horowitz, L. W., Lamarque, J.-F., Lin, M., Prather, M. J., Young, P. J., Bergmann, D., Cameron-Smith, P. J., Cionni, I., Collins, W. J., Dalsøren, S. B., Doherty, R., Eyring, V., Faluvegi, G., Folberth, G. A., Josse, B., Lee, Y. H., MacKenzie, I. A., Nagashima, T., van Noije, T. P. C., Plummer, D. A., Righi, M., Rumbold, S. T., Skeie, R., Shindell, D. T., Stevenson, D. S., Strode, S., Sudo, K., Szopa, S., and Zeng, G.: Preindustrial to present-day changes in tropospheric hydroxyl radical and methane lifetime from the Atmospheric Chemistry and Climate Model Intercomparison Project (ACCMIP), Atmospheric Chemistry and Physics, 13, 5277–5298, https://doi.org/10.5194/acp-13-5277-2013, 2013.

Nault, B. A., Laughner, J. L., Wooldridge, P. J., Crounse, J. D., Dibb, J., Diskin, G., Peischl, J., Podolske, J. R., Pollack, I. B., Ryerson, T. B., Scheuer, E., Wennberg, P. O., and Cohen, R. C.: Lightning NOx Emissions: Reconciling Measured and Modeled Estimates With Updated NO Chemistry, Geophysical Research Letters, 44, 9479–9488, https://doi.org/10.1002/2017GL074436, 2017.

Ott, L. E., Pickering, K. E., Stenchikov, G. L., Allen, D. J., DeCaria, A. J., Ridley, B., Lin, R.-F., Lang, S., and Tao, W.-K.: Production of lightning NO and its vertical distribution calculated from three-dimensional cloud-scale chemical transport model simulations, Journal of Geophysical Research: Atmospheres, 115, D04 301, https://doi.org/https://doi.org/10.1029/2009JD011880, 2010.

Pawar, S. D., Lal, D. M., and Murugavel, P.: Lightning characteristics over central India during Indian summer monsoon, Atmospheric Research, 106, 44–49, https://doi.org/10.1016/j.atmosres.2011.11.007, 2012a.

Pawar, V., Pawar, S. D., Beig, G., and Sahu, S. K.: Effect of lightning activity on surface NOx and O_3 over a tropical station during pre-monsoon and monsoon seasons, Journal of Geophysical Research: Atmospheres, 117, D05 310, https://doi.org/10.1029/2011JD016930, 2012b.

Pérez-Invernón, F. J., Gordillo-Vázquez, F. J., Huntrieser, H., Jöckel, P., and Bucsela, E. J.: Sensitivity of climate-chemistry model simulated atmospheric composition to lightning-produced NOx parameterizations based on lightning frequency, EGUsphere, 2024, 1–26, https://doi.org/10.5194/egusphere-2024-3348, 2024.

Pickering, K. E., Wang, Y., Tao, W.-K., Price, C., and Müller, J.-F.: Vertical distributions of lightning NOx for use in regional and global chemical transport models, Journal of Geophysical Research: Atmospheres, 103, 31 203–31 216, https://doi.org/10.1029/98JD02651, 1998.

Price, C. and Rind, D.: A simple lightning parameterization for calculating global lightning distributions, Journal of Geophysical Research: Atmospheres, 97, 9919–9933, https://doi.org/10.1029/92JD00719, 1992.

Price, C. and Rind, D.: What determines the cloud-to-ground lightning fraction in thunderstorms?, Geophysical Research Letters, 20, 463–466, https://doi.org/10.1029/93GL00226, 1993.

Price, C. and Rind, D.: Modeling global lightning distributions in a general circulation model, Monthly Weather Review, 122, 1930–1939, https://doi.org/10.1175/1520-0493(1994)122<1930:MGLDIA>2.0.CO;2, 1994.

Price, C., Penner, J., and Prather, M.: NOx from lightning: 1. Global distribution based on lightning physics, Journal of Geophysical Research: Atmospheres, 102, 5929–5941, https://doi.org/10.1029/96JD03504., 1997a.

Price, C., Penner, J., and Prather, M.: NOx from lightning: 2. Constraints from the global atmospheric electric circuit, Journal of Geophysical Research: Atmospheres, 102, 5943–5951, https://doi.org/10.1029/96JD02551, 1997b.

Pun, B. K. and Seigneur, C.: Investigative modeling of new pathways for secondary organic aerosol formation, Atmospheric Chemistry and Physics, 7, 2199–2216, https://doi.org/10.5194/acp-7-2199-2007, 2007.

Ren, Y., Xu, W., and Fu, J.: Characteristics of intracloud lightning to cloud-to-ground lightning ratio in thunderstorms over Eastern and Southern China, Atmospheric Research, 300, 107 231, https://doi.org/10.1016/j.atmosres.2024.107231, 2024.

Schumann, U. and Huntrieser, H.: The global lightning-induced nitrogen oxides source, Atmospheric Chemistry and Physics, 7, 3823–3907, https://doi.org/10.5194/acp-7-3823-2007, 2007.

Tiedtke, M.: A comprehensive mass flux scheme for cumulus parameterization in large-scale models, Monthly Weather Reviews, 117, 1779–1800, https://doi.org/10.1175/1520-0493(1989)117<1779:ACMFSF>2.0.CO;2, 1989.

Tost, H., Jöckel, P., and Lelieveld, J.: Lightning and convection parameterisations uncertainties in global modelling, Atmospheric Chemistry and Physics, 7, 4553–4568, https://doi.org/10.5194/acp-7-4553-2007, 2007.

Troen, I. and Mahrt, L.: A simple model of the atmospheric boundary layer: Sensitivity to surface evaporation, Boundary-Layer Meteorology, 37, 129–148, https://doi.org/10.1007/BF00122760, 1986.

Uman, M. A.: The lightning discharge, Courier Corporation, 2001.

van der A, R. J., Eskes, H. J., Boersma, K. F., van Noije, T. P. C., Van Roozendael, M., De Smedt, I., Peters, D. H. M. U., and Meijer, E. W.: Trends, seasonal variability and dominant NOx source derived from a ten year record of NO2 measured from space, Journal of Geophysical Research: Atmospheres, 113, D04 302, https://doi.org/10.1029/2007JD009021, 2008.

van Leer, B.: Towards the ultimate conservative difference scheme: IV. A new approach to numerical convection, Journal of Computational Physics, 23, 276–299, https://doi.org/10.1016/0021-9991(77)90095-X, 1977.

Verma, S., Yadava, P. K., Lal, D. M., Mall, R. K., Kumar, H., and Payra, S.: Role of Lightning NOx in Ozone Formation: A Review, Pure and Applied Geophysics, 178, 1425–1443, https://doi.org/10.1007/s00024-021-02710-5, 2021.

von Kuhlmann, R., Lawrence, M. G., Crutzen, P. J., and Rasch, P. J.: A model for studies of tropospheric ozone and nonmethane hydrocarbons: Model description and ozone results, Journal of Geophysical Research: Atmospheres, 108, https://doi.org/10.1029/2002JD002893, 2003.

Vonnegut, B.: Some facts and speculations concerning the origin and role of thunderstorm electricity, pp. 224–241, American Meteorological Society, https://doi.org/10.1007/978-1-940033-56-3_11, 1963.

Voulgarakis, A., Naik, V., Lamarque, J.-F., Shindell, D. T., Young, P. J., Prather, M. J., Wild, O., Field, R. D., Bergmann, D., Cameron-Smith, P., Cionni, I., Collins, W. J., Dalsøren, S. B., Doherty, R. M., Eyring, V., Faluvegi, G., Folberth, G. A., Horowitz, L. W., Josse, B., MacKenzie, I. A., Nagashima, T., Plummer, D. A., Righi, M., Rumbold, S. T., Stevenson, D. S., Strode, S. A., Sudo, K., Szopa, S., and Zeng, G.: Analysis of present day and future OH and methane lifetime in the ACCMIP simulations, Atmospheric Chemistry and Physics, 13, 2563–2587, https://doi.org/10.5194/acp-13-2563-2013, 2013.

Wesely, M.: Parameterization of Surface Resistances to Gaseous Dry Deposition in Regional-Scale Numerical Models, Atmospheric Environment, 23, 1293–1304, https://doi.org/10.1016/0004-6981(89)90153-4, 1989.

Wild, O., Zhu, X., and Prather, M. J.: Fast-J: Accurate Simulation of In- and Below-Cloud Photolysis in Tropospheric Chemical Models, Journal of Atmospheric Chemistry, 37, 245–282, https://doi.org/10.1023/A:1006415919030, 2000.

Williams, E. R.: Large-scale charge separation in thunderclouds, Journal of Geophysical Research: Atmospheres, 90, 6013–6025, https://doi.org/10.1029/JD090iD04p06013, 1985.

Wu, Y., Pour-Biazar, A., Koshak, W., and Cheng, P.: LNOx emission model for air quality and climate studies using satellite lightning mapper observations, Journal of Geophysical Research: Atmospheres, 128, e2022JD037 406, https://doi.org/10.1029/2022JD037406, 2023.

Xu, M., Qie, X., Zhao, C., Yuan, S., Li, J., Tao, Y., Shi, G., Pang, W., and Shi, L.: Distribution of lightning spatial modes and climatic causes in China, Atmospheric and Oceanic Science Letters, 16, 100 338, https://doi.org/10.1016/j.aosl.2023.100338, 2023.

Young, P. J., Archibald, A. T., Bowman, K. W., Lamarque, J.-F., Naik, V., Stevenson, D. S., Tilmes, S., Voulgarakis, A., Wild, O., Bergmann, D., Cameron-Smith, P., Cionni, I., Collins, W. J., Dalsøren, S. B., Doherty, R. M., Eyring, V., Faluvegi, G., Horowitz, L. W., Josse, B., Lee, Y. H., MacKenzie, I. A., Nagashima, T., Plummer, D. A., Righi, M., Rumbold, S. T., Skeie, R. B., Shindell, D. T., Strode, S. A., Sudo, K., Szopa, S., and Zeng, G.: Pre-industrial to end 21st century projections of tropospheric ozone from the Atmospheric Chemistry and Climate Model Intercomparison Project (ACCMIP), Atmospheric Chemistry and Physics, 13, 2063–2090, https://doi.org/10.5194/acp-13-2063-2013, 2013.

Zhang, D., Cummins, K. L., Lang, T. J., Buechler, D., and Rudlosky, S.: Performance Evaluation of the Lightning Imaging Sensor on the International Space Station, Journal of Atmospheric and Oceanic Technology, 40, 1063–1082, https://doi.org/10.1175/JTECH-D-22-0120.1, 2023.

Zhang, L., Gong, S., Padro, J., and Barrie, L.: A size-segregated particle dry deposition scheme for an atmospheric aerosol module, Atmospheric Environment, 35(3), 549–560, https://doi.org/10.1016/S1352-2310(00)00326-5, 2001.

Zhao, C., Wang, Y., Choi, Y., and Zeng, T.: Summertime impact of convective transport and lightning NOx production over North America: modeling dependence on meteorological simulations, Atmospheric Chemistry and Physics, 9, 4315–4327, https://doi.org/www.atmos-chem-phys.net/9/4315/2009/, 2009.

Zhao, Y., Saunois, M., Bousquet, P., Lin, X., Hegglin, M. I., Canadell, J. G., Jackson, R. B., and Zheng, B.: Reconciling the bottom-up and top-down estimates of the methane chemical sink using multiple observations, Atmospheric Chemistry and Physics, 23, 789–807, https://doi.org/10.5194/acp-23-789-2023, 2023.

Ziemke, J., Chandra, S., Duncan, B., Froidevaux, L., Bhartia, P., Levelt, P., and Waters, J.: Tropospheric ozone determined from Aura OMI and MLS: Evaluation of measurements and comparison with the Global Modeling Initiative's Chemical Transport Model, Journal of Geophysical Research: Atmospheres, 111, https://doi.org/10.1029/2006JD007089, 2006.